Holocene glacier fluctuations and environmental changes in sub-Antarctic South Georgia inferred from a sediment record from a coastal inlet

Sonja Berg, Institute of Geology and Mineralogy, University of Cologne, 50674 Cologne, Germany

Duanne A. White, Institute for Applied Ecology, University of Canberra, ACT, Australia, 2601.

Sandra Jivcov, Institute of Geology and Mineralogy, University of Cologne, 50674 Cologne, Germany

Martin Melles, Institute of Geology and Mineralogy, University of Cologne, 50674 Cologne, Germany

Melanie J. Leng, NERC Isotopes Geosciences Facilities, British Geological Survey, Keyworth, Nottingham NG12 5GG, UK & School of Biosciences, Centre for Environmental Geochemistry, The University of Nottingham, Sutton Bonington Campus, Leicestershire LE12 5RD, UK

Janet Rethemeyer, Institute of Geology and Mineralogy, University of Cologne, 50674 Cologne, Germany

Claire Allen (BAS) British Antarctic Survey, High Cross, Madinley Road, Cambrige UK

Bianca Perren (BAS) British Antarctic Survey, High Cross, Madinley Road, Cambrige UK

Ole Bennike, Geological Survey of Denmark and Greenland, Copenhagen, Denmark.

Finn Viehberg, Institute of Geology and Mineralogy, University of Cologne, 50674 Cologne, Germany

Corresponding Author:

Sonja Berg,

Institute of Geology and Mineralogy, University of Cologne

Zuelpicher Strasse 49a, 50674 Cologne, Germany

Email: sberg0@uni-koeln.de; Phone ++49 221 470 2540

Abstract

The sub-Antarctic island of South Georgia provides terrestrial and coastal marine records of climate variability, which are crucial for the understanding of the drivers of Holocene climate changes in the sub-Antarctic region. Here we investigate a sediment core (Co1305) from a coastal inlet on South Georgia using elemental, lipid biomarker, diatom and stable isotope data to infer changes in environmental conditions and to constrain the timing of Late glacial and Holocene glacier fluctuations. Due to the scarcity of terrestrial macrofossils and the presence of re-deposited and relict organic matter in the sediments, age control for the record was obtained by compound-specific radiocarbon dating of mostly marine derived *n*-C_{16} fatty acids. A basal till layer recovered in Little Jason Lagoon was likely deposited during an advance of local glaciers during the Antarctic cold reversal. After glacier retreat an oligotrophic lake occupied the site, which transitioned to a marine inlet around 8.0±0.9 ka due to relative sea level rise. From 7.0±0.6 to 4.0±0.4 ka reduced vegetation coverage in the catchment as well as high siliciclastic input and deposition of ice rafted debris indicate glacier advances in the terrestrial catchment and likely in the adjacent fjord. A second, less extensive period of glacier advances occurred in the late Holocene, after 1.8±0.3 ka.

Keywords

South Georgia, Holocene, glacier advance, compound-specific radiocarbon analysis, marine sediments, relative sea level

INTRODUCTION

Glacier mass balance and therefore glacier extent directly responds to atmospheric conditions. Land terminating mountain glaciers are largely controlled by summer temperature, which effects ablation in the summer season (Oerlemans et al., 2005). On the sub-Antarctic islands atmospheric drying likely is an additional driver for glacier retreat, which is presently observed (Gordon et al., 2008; Favier et al., 2016). In this respect the temporal and spatial pattern of glacier fluctuations can provide sensitive measure of the climatic history. In the sub-Antarctic region between 40° and 60°S the position and strengths of the Southern Hemisphere Westerly Winds (SHWW) controls the distribution of precipitation (e.g. Lamy et al., 2010) and influences ocean circulation by supporting wind-driven upwelling of deep water in the Southern Ocean south of the polar front (PF) (e.g. Toggweiler, 2009, Fig. 1). The island of South Georgia (54-55°S, 36-38°W, Figs. 1 and 2A) is one of the few sites in the Southern Hemisphere mid-lower latitudes that provide terrestrial and coastal marine records of former glacier extent. This makes South Georgia a prime study site to better understand the drivers of Holocene climate changes in the sub-Antarctic region.

Correlation of glacier deposits from different sites on South Georgia is mainly based on relative weathering and soil development studies (Clapperton et al., 1989; Bentley et al., 2007; White et al., 2017). Continuous records from lakes and marine inlets can complement the geomorphological evidence by providing high-resolution chronological constraints on both glaciation history and climate fluctuations. Here we present a sediment record of Holocene environmental changes from a marine inlet at the northern shore of South Georgia. We use a combination of elemental, biomarker, diatom and stable isotope data to infer changes in glacier extent and environmental conditions in the terrestrial and marine catchments of the inlet. The results provide information on the timing of the deglaciation and Holocene glacier advances and retreats, thereby improving the picture of the temporal development of land-based glaciers on South Georgia. We compare our reconstructions to records from the Antarctic Peninsula Region and from southern South America.

STUDY AREA

South Georgia has a maritime climate with a mean annual temperature of +1.9°C (Grytviken weather station, Trouet and Van Oldenborgh, 2013). At present the central mountain range is covered by extensive ice fields, feeding numerous outlet glaciers, some of which presently terminate at sea level as tide-water glaciers. Small local glaciers with source areas lower than 600 m above sea level (a.s.l.) exist in cirques and on plateaus at lower altitudes (Clapperton, 1990).

Geomorphological features on land and adjacent marine and fjord landforms indicate that the island was extensively glaciated in the past (Clapperton et al., 1989; Bentley et al., 2007; Graham et al., 2008; Hodgson et al., 2014a; Barlow et al., 2016; White et al., 2017). Exposure dating of glacial erratics suggests that the recession of a last glacial maximum (LGM) ice cap exposed lower elevations around 16±1.5 ka (White et al., 2017). A lake record from the Stromness Bay area points to biogenic lake sedimentation starting around 18.6 ka (Rosqvist et al., 1999, Fig. 2A). The initial ice retreat was followed by an ice re-advance into the fjords during the Antarctic cold reversal (ACR, 14.7 -13 ka; Pedro et al., 2016; Graham et al., 2017). Deglaciation of low altitude sites was well under way in the early Holocene, documented by the onsets of biogenic sedimentation in lakes and peat lands (Van der Putten and Verbruggen, 2005; Hodgson et al., 2014b). In the mid-Holocene ('neoglacial') widespread growth of glaciers on South Georgia occurred (e.g., Clapperton et al., 1989; Bentley et al., 2007; White et al., 2017). Tidewater glaciers advanced into the fjords on the north-western side of the island (Bentley et al., 2007) and smaller land-terminating glaciers expanded down to lower altitudes (e.g., Clapperton et al., 1989; Clapperton, 1990; White et al., 2017). In the late Holocene South Georgia experienced another period of glacier advances (e.g., Rosqvist et al., 2003; Bentley et al., 2007; Roberts et al., 2010, van der Bilt et al., 2017). Glacier advances were less extensive than in the mid-Holocene and showed variability on centennial time scales (van der Bilt et al., 2017).

Our coring site was located in a coastal inlet (Little Jason Lagoon) on the northwestern shore of Lewin Peninsula (Fig. 2A). At present, the inlet is connected with Cumberland West Bay over a 0.5 to 1.5 m deep sill. This results in marine conditions in the inlet and likely leads to sediment supply from suspensions and ice rafted debris (IRD) originating from glaciers calving into Cumberland West Bay to the south-west of Little Jason Lagoon (e.g., Neumayer Glacier, Fig. 2A,B). The maximum water depth in the inlet is c. 24 m (Melles et al., 2013). Several small streams enter Little Jason Lagoon (Fig. 2B), with runoff being subject to seasonal changes with a peak during the snow-melt in austral summer. Areas below *c.* 200 m a.s.l. are covered by vegetation, which is characterized by tussock grass (*Parodiochloa flabellata*), other grasses (*Festuca contracta* and *Deschampsia antarctica*), subshrubs (*Acaena* spp.), rushes (*Juncus* spp. and *Rostkovia magellanica*), and mosses (Greene, 1964). The catchment of Little Jason Lagoon (highest elevation is Jason Peak, 570 m a.s.l) is presently free of permanent ice or snowfields. Moraine ridges and debris deposits point to periods of expanded local mountain glaciers in the catchment of the inlet (Fig. 2B). Clapperton et al. (1989) identified five stages of glacier advances on South Georgia. The oldest moraine ridges around Little Jason Lagoon document glaciers reaching down to modern sea level and correlate to “stage 3” sensu Clapperton et al. (1989). The deposits have weathering characteristics that are broadly consistent with a late glacial formation (White et al., 2017). Another ice advance is represented by a suite of glacial deposits, which are the remnants of cirque glaciers extending down to c. 30 m a.s.l. (White et al., 2017; Fig. 2B) and correlate with a mid-Holocene advance (“stage 4” Clapperton et al., 1989). The youngest, late Holocene (“stage 5” deposits; Clapperton et al., 1989) glacier advance was restricted to small mountain glaciers, which formed in the upper catchment above 250 m a.s.l. (White et al., 2017; Fig. 2B).

MATERIALS AND METHODS

Coring

Sediment coring on Little Jason Lagoon was carried out in March 2013 within the scope of the expedition ANT XXIX/4 of RV *Polarstern* (Melles et al., 2013). Coring was conducted in the deepest part of the lagoon from a platform. A gravity corer (UWITEC Ltd., Austria) was used for sampling of the uppermost sediment decimetres and the sediment–water interface. Deeper sediments were sampled using a percussion piston corer (UWITEC Ltd., Austria). The piston cores retrieved from LJL overlap by about 1 m. The final core composite of core Co1305 has a length of 11.04 m; it consists of seven gravity and piston cores, which were correlated on the basis of core descriptions and analytical data (XRF-elemental scans and water content) in overlapping core segments.

Core processing and physical properties

The sediment cores were stored at 4°C until opening in the laboratory. One core half was used for non-destructive analysis, i.e. line-scan imaging with a multi sensor core logger (GeoTek, UK), X-Ray Fluorescence (XRF) scanning (see below), and core description. For analyses of discrete samples, the working half of the composite core was subsampled in 2 cm slices. The sediment samples were freeze-dried and the water content was determined by weight loss during freeze-drying.

As a proxy for ice-rafted debris (IRD), the number of particles >1 mm in diameter was quantified for 47 samples. For that purpose, 6 to 25 g of wet sediment (corresponding to subsampled 2 cm sediment slices) were wet sieved on a 1 mm steel mesh sieve. The number of mineral grains retained on the sieve were counted and normalized to the dry sediment weight of the respective samples.

Elemental analysis

The chemical composition of the sediment core was investigated at 2 mm resolution by XRF scanning, using an ITRAX XRF core scanner (Cox Ltd.; Croudace et al., 2006). Measurements were performed with a chromium X-ray tube with 30 mA, 30 kV, and an exposure time of 20 sec. Results are given as counts per second (cps), which is a semi-quantitative measure of element concentration, or as element count ratios.

Furthermore, quantitative elemental analyses of total sulphur (S) and total carbon (C) were conducted on 86 aliquots of ground sediment samples with a Vario Micro Cube combustion elemental analyser (Elementar, Germany) and total inorganic carbon (TIC) was quantified on parallel samples with a DIMATOC 200 (DIMATEC Corp.).

Stable isotope analysis

The $\delta^{13}C$ values of the bulk organic matter (OM) and the corresponding C/N ratios can be indicative for the sources of OM, i.e. they can be used to distinguish freshwater, terrestrial and marine sources of OM and hence indicate depositional environments (e.g. Leng and Lewis, 2017). $\delta^{13}C$ ratios and the C/N concentrations were determined on 75 samples with equal sampling intervals. In preparation of the measurements, freeze-dried sediment samples were treated with 5% HCl to remove any $CaCO_3$ and then washed thrice in 500 ml deionised water. After drying at 40°C the material was ground to a fine powder using an agate pestle and mortar. $\delta^{13}C$ analyses were performed by combustion in a Costech ECS4010 Elemental Analyser (EA) on-line coupled to a VG TripleTrap (plus secondary cryogenic trap) and Optima dual-inlet mass spectrometer. We use the C and N values obtained with the EA during the isotope analysis for calculating the C/N ratio. %C analyses were calibrated against an Acetanilide standard. The $\delta^{13}C$ values were calculated to the VPDB scale using a within-run laboratory standard (BROC2) calibrated against NBS-19 and NBS-22. Replicate analysis of well-mixed samples indicated a precision of <0.1‰ (1 SD).

Diatom analysis

Diatom analysis was carried out on 12 samples with equal sampling intervals to determine the depositional environment, hence to distinguish lacustrine from marine conditions. Quantitative preparation of diatom slides was conducted on 0.01 to 0.025 grams of dried sediment following the settling method of Scherer (1994). Diatom counting was carried out on a light microscope at ×1000 magnification. Where possible, a minimum of 300 specimens were counted and identified to species or genus level. Taxonomic classification follows that of Hasle and Syvertsen (1997), supplemented with descriptions of Antarctic species by Krebs (1983), Johansen and Fryxell (1985), and Scott and Thomas (2005).
Diatom species were grouped into freshwater diatoms (e.g. *Achnanthidium minutissimum, Amphora veneta, Craticula* sp*. Cymbella cistula, Discostella stelligera, Diploneis* sp*. Discostella stelligera, Fragilaria capucina, Fragilaria germainii, Fragilaria tenera,* with *D. stelligera* and small Fragilariaceae, such as *Staurosirella* sp.*, Psuedostaurosira* spp*.,* etc. being the most dominant ones) and marine diatoms (e.g. *Chaetoceros hyalocheate* vegetative cells, *Chaetoceros* resting spores*, Thalassiosira antarctica, Odontella litigiosa* and *Fragilariopsis* spp.). The remainder of the diatom species comprise marine benthic and brackish taxa, including *Cocconeis* spp. and *Navicula* spp., which have been merged, since there is considerable overlap between their habitats. A summary of diatom species identified in sample of core Co1305 is given in the supplementary table S1.

Lipid biomarker analysis

The concentration and distribution of *n*-alkanes with chain lengths of 25 to 35 carbon atoms (C_{25}-C_{35}) were analysed in 33 samples from 5 cm thick layers sampled in 50 cm intervals from core Co1305. The high molecular weight (HMW) *n*-alkanes are compounds of leaf waxes of higher land plants and thus can be used as terrestrial biomarkers in sediments (review by Pancost et al., 2004). The *n*-alkanes were extracted from the sediment samples by accelerated solvent extraction (ASE 300, Thermo, USA) using dichloromethane and methanol (DCM, MeOH; 9:1, v/v at 120°C, 75 bar) yielding total extractable lipids (TLE). The TLE was saponified with 0.5 M KOH in MeOH and water (9:1, v/v) at 80°C for 2 h and desulfurized using activated copper. Neutral lipids (NL) were extracted from TLE with dichloromethane by liquid-liquid phase separation from which *n*-alkanes were purified by column chromatography (SiO_2, deactivated, mesh 60) and elution with hexane. Individual compounds were identified and quantified by gas chromatograph (GC Agilent 7890B, Agilent Technologies, USA) with a flame ionization detector (FID) and using an external standard (*n*-alkanes C_{21} to C_{40}, 40 mg/l each; Sigma Aldrich). The GC was equipped with a 50 m DB5 MS column (0.2 mm i.d. and 0.33 µm film thickness by Agilent Technologies, USA). Concentrations are normalized to the total organic carbon (TOC) content of the respective samples (µg/g TOC), which was analysed on aliquots of the original sediment samples with a DIMATOC 200 (DIMATEC Corp.).

In living plants, odd numbered *n*-alkanes dominate over even numbered homologues (Eglinton and Hamilton, 1963). When plant material is degraded in soils or peat deposits, e.g. by microbial activity, the even numbered homologues become more abundant. We calculated the carbon preference index (CPI) for odd over even dominance for C_{25}-C_{35} (after Marzi et al., 1993) to use it as a source indicator as well as a measure of degradation of the organic material.

Radiocarbon dating and core chronology

For age assignment of the sediment sequence we conducted radiocarbon (^{14}C) analysis on different organic materials. Macroscopic plant fossils were mainly preserved in the lower part of the core and could be picked from 6 depths. In the upper part (105 cm depth) a kelp fragment and a mollusc shell were found, which were used for ^{14}C-analysis. A second carbonate fossil could be dated from 264 cm depth. If no macrofossil could be selected, bulk organic carbon (OC) was dated (8 samples throughout the core). For the determination of a present day local marine reservoir age we dated a recent carbonate shell of a marine mollusc, which was sampled on the beach of Grytviken. Since bulk OC contains a mixture of OM from various sources, ^{14}C ages do not necessarily reflect the sedimentation age. In the setting of Little Jason Lagoon OM is not only derived from autochthonous marine production, but also contains older, (glacially) re-worked carbon as well as terrestrial OM from plant remains and soils. We thus additionally use compound-specific ^{14}C analysis of lipid biomarkers to better constrain the source and time of delivery from land into the sediment of the dated material. Since biomarkers derived from terrestrial vascular plants may be considerably older because of intermediate storage in soils (e.g. Drenzek et al., 2007), we use the *n*-C_{16} FA , which is a common compound of aquatic and marine biomass (e.g. phytoplankton, Volkman et al., 1980). Previous studies in this region have shown that *n*-C_{16} FA ages reflect the value of dissolved inorganic carbon (DIC) during OM formation (Ohkuchi and Eglinton, 2008) and therefore have the potential to provide the sediment age (e.g., Uchida et al., 2001).

Sample preparation for ^{14}C analysis was done using standard methods (Rethemeyer et al. (2013). Briefly, bulk OC and macro fossil samples were decarbonised with acid and converted into CO_2 by combustion. Carbonate samples were leached with acid and subsequently converted into CO_2 with phosphoric acid. The CO_2 was transformed into graphite cathodes using the automated graphitization equipment AGE (Ionplus, Switzerland).

AMS measurements were carried out at the CologneAMS facility (University of Cologne, Germany; Dewald et al., 2013).

For compound-specific radiocarbon analyses FAs were separated from TLE after acidification with HCl by liquid-liquid phase separation and subsequent open column chromatography as described in Höfle et al. (2013). FAs were transferred to fatty acid methyl esters (FAMEs) using MeOH with known ^{14}C content to correct the results for the carbon added. The purification of the n-C_{16} FA was conducted by preparative capillary gas chromatography. The system consists of a GC (7680 Agilent Technologies, USA) equipped with a CIS 4 injection system (Gerstel, Germany), and is coupled with a preparative fractionation collector (PFC; Gerstel, Germany). Chromatographic separation was done with a "megabore" ultra-low bleed capillary column (30 m, 0.53 mm I.D.; Restek, USA) and trapping of n-C_{16} FA with the PFC was achieved at room temperature. The purity and quantity of trapped compounds was analysed by GC-FID (on-column, Agilent 7890B, Agilent Technologies, USA). The isolated n-C_{16} FA was transferred into quartz tubes with copper oxide (CuO) and silver (Ag) added and vacuum-sealed. All quartz tubes, CuO and Ag were pre-combusted (900°, 4h) prior to use. Samples were combusted at 900°C to form CO_2. The CO_2 was purified cryogenically and analysed on a MICADAS AMS system using its gas ion source (ETH Zurich, Switzerland, Wacker et al., 2010). Compound ages were corrected for process blank and methylation by mass balance calculation following the procedure described by Rethemeyer et al. (2013).

RESULTS

Lithology, sediment composition and environmental settings

Based on the lithology, the elemental, biomarker, and diatom compositions, and the stable isotope data the 11.04 m long core composite Co1305 was divided into four distinct units (Fig. 3J). Since TIC values were not distinguishable from background in all analysed samples, we considered the C content to be similar to TOC concentration.

Unit I (1104-1042 cm)

Unit I consists of a grey diamicton, which contains a mixture of sand, silt and clay as well as interspersed rock fragments with diameters of up to several centimetres. A very low water content of around 14wt% in the lower part (1104 to 1066 cm) suggests overconsolidation (Fig. 3G). The sediment becomes successively wetter and less coarse-grained in the uppermost ca. 20 cm. These sediment characteristics point to deposition in a sub-glacial environment (basal till), possibly passing into a pro-glacial environment in the upper part (waterlain till) (e.g. Eyles et al., 1991).

A sub-glacial to pro-glacial deposition of unit I is supported by the elemental and biomarker data. The C and S contents throughout the unit with <0.3wt% and <0.2wt%, respectively, are minimal (Fig. 3F). A specific source of OM cannot clearly be assigned based on the $\delta^{13}C$ values and C/N ratios (Fig. 4). $\delta^{13}C$ values of –26.0±0.1‰ could originate from lacustrine or land-plant sources, while the low and variable C/N ratios (6.5±1.0) may reflect a bacterial origin (Lamb et al., 2006; Leng and Lewis 2017). From one sample (1048 cm depth) *n*-alkanes were extracted (24 µg/g TOC) (Fig. 3E), which were dominated by homologues of C_{29} and C_{31} carbon atoms and had a CPI of 5.7 characteristic for soil-derived, slightly humified OM (Andersson and Meyers 2012; Angst et al., 2016) (Fig. 5). The OM in unit I most likely originates from reworked allochthonous sources.

Unit II (1042-996 cm)

Unit II consists of finely laminated silt and clay with some irregularly interspersed rock fragments and mineral grains in the >1 mm fraction (Fig. 3C). These coarse-grained particles in a very fine-grained matrix most likely represent ice-rafted debris (IRD; Grobe, 1987 and refs. therein), originating either from icebergs (as supraglacial, englacial or subglacial debris) or from lake ice floats (due to basal freeze-on or surface spill close to the shore) as suggested for Arctic lake and marine environments (Smith, 2000; Sakamoto et al., 2005) . The fine-grained lamination furthermore points to a low energetic depositional environment. In the lower part of unit II laminae are formed by alternating proportions of dispersed OM and siliciclastic components. Above 1026 cm interspersed macroscopic moss fragments, form discrete sediment layers. There, significant biogenic production and accumulation is also evidenced by C and S contents of c. 1.2wt% (Fig. 3F).

Diatom concentrations in unit II have a mean value of 7 million valves per gram sediment (Mv/g; Table S1). The diatom *Discostella stelligera* dominates during this interval. It is a freshwater planktonic taxon, which is common in oligotrophic lakes in Greenland and elsewhere in the Arctic (e.g. Saros and Anderson, 2014). A freshwater origin of parts of the OM in unit II is also reflected by low $\delta^{13}C$ values (–28.1±0.5‰) and C/N ratios of 8.5±0.3 (Fig. 4). Concentrations of leaf wax *n*-alkanes range from 73 to 115 µg/g TOC (95±16 µg/g TOC, Fig. 3E) and CPI values around 9 (Fig. 5) reflect input of less decomposed soil OM than in unit I and larger contributions of higher terrestrial plants into the lake.

Unit III (996-978 cm)

Sediments in unit III are finely laminated and fine grained (silt and clay), suggesting that the low-energy environment of unit II persisted during the formation of unit III. The same holds true for the lack of bioturbation, possibly due to a reduced ventilation of the water column.

One sample was checked for mineral grains in the >1 mm sieve fraction (from 986 cm depth) and did not contain any IRD (Fig. 3C).

The diatom assemblage in the one sample analysed from unit III (986 cm, Fig. 3I) contains 3% of counted diatoms from the freshwater group, whereas brackish/benthic and marine diatoms contribute almost equal amounts of 41 and 56%, respectively (Fig. 3I). This indicates a change to more saline conditions, likely due to a marine ingression. A transition from lacustrine to marine conditions is supported by a significant increase in $\delta^{13}C$ values throughout unit III (Figs. 3H and 4), which is indicative for the incorporation of marine OM (Leng and Lewis, 2017). The transition is accompanied by an increase in S in the sediments of unit III, which reaches a maximum of 4wt% at 994 cm depth.

The C content in unit III increases, ranging from 1.9 to 2.5wt% (Fig. 3F). $\delta^{13}C$ values point to autochthonous origin of OM, e.g. from diatoms and other phytoplankton groups (Figs. 3H and 4). However, larger contributions of terrestrial OM are indicated by slightly higher C/N ratios in unit III (9.0-10.9) compared to unit II (8.5±0.3; Figs. 3H and 4). The input of higher plant-derived OM is supported by a maximum concentration of C_{25}-C_{35} *n*-alkanes in the two samples analysed from unit III (634 and 480 µg/g TOC; Fig. 3E) and by the high CPI values of 13, which are within the range of fresh plant material (Fig. 5).

Unit IV (978-0 cm)

Sediments of unit IV are layered at cm-scale. The material is generally fine grained (silt and clay) with changing minor proportions of sand and gravelly IRD (Fig. 3C). This is also reflected by cm-scale variations in Ti, which is exclusively of minerogenic origin and therefore indicates recurring changes in siliclastic input (Fig 3D). Changes in the inorganic composition of the sediments in unit IV are suggested by changes in the Si/Ti-ratio (Fig. 3D). In contrast to Ti, Si can also be derived from biogenic silica, produced by diatoms and sponges. Changes in the Si/Ti-ratio may therefore reflect changes in the proportion of biogenic silica and siliclastic material. C concentrations in unit IV range from 0.9 to 3.3wt% (mean 2.0±0.5wt%) with lowest organic carbon contents between 938-714 cm depth (Fig. 3F).

The dominance of marine diatoms (84-93%, Fig. 3I) throughout unit IV indicates full marine conditions. The frustules are well preserved and *Chaetoceros* resting spores (82-93%) dominate the assemblage, suggesting high productivity within a seasonally stratified water column (Hargraves and French, 1983). The benthic species in unit IV are frequently found in the Antarctic Peninsula region. They are cold-water taxa not specifically associated with sea-ice (Al-Handel and Wolff, 2008 a, b; Lange et al., 2007). Marine conditions are also indicated by high $\delta^{13}C$ values (–20.3±0.6‰) and low C/N ratios (7.4±0.3), which are typical for OM derived from marine algae (Fig. 4). Additional indication comes from the occurrence of marine macro algae (kelp), in particular above 502 cm (Fig. 3A).

Concentration of land-plant derived *n*-alkanes, ranging from 46 to 347 µg/g TOC (with a mean of 143±67 µg/g TOC) and CPI values from 11 to 21 (Fig. 5) reflect high but variable inputs of land-plant derived material into the inlet (Fig. 3E).

Core chronology

A total of 24 ^{14}C ages was obtained for core Co1305. Ages range from 660±40 ^{14}C yr BP (plant fossil in 10 cm depth) to 14170±70 ^{14}C yr BP for bulk OC from the base of unit II (Figs. 3B and 6A, Table 1). Bulk OC ages become successively older with depth, except for one data point. However, ^{14}C ages of bulk OC are significantly older than those of carbonates and plant remains from similar or lower core levels (Fig. 6A) suggesting that the sediments contain high and variable proportions of older C and does not reflect the actual age of sedimentation.

The ^{14}C ages of n-C_{16} FAs are younger than those in bulk OC and they are in good agreement with ^{14}C ages of the kelp and carbonate macrofossils selected from 105 cm core depth suggesting a common marine source (Fig. 6A, Table 1). The un-calibrated ^{14}C ages of two mosses dated from unit III are c. 800 years older than the n-C_{16} FA from the corresponding core depth (Fig. 6A, Table 1). Much older plant fossils, which probably do not reflect sediment age, were also found in other lake sediment records from South Georgia (Strother et al., 2014; van der Bilt et al., 2016). The age-offset likely results from long transport times or intermediate storage in the catchment prior to deposition in the sediment. In Little Jason Lagoon the n-C_{16} FA age likely best reflects the sediment age by providing a ^{14}C signal of aquatic production rather than of potentially pre-aged terrestrial OM.

Due to the scarcity of datable macrofossils in the sediments and the potentially reworked origin of terrestrial OM in Little Jason Lagoon, we also use n-C_{16} FA ages for the age-depth model of core Co1305. This, however, requires correction for the marine reservoir effect. Benthic foraminifers from the shelf off South Georgia provided ^{14}C ages of 1100 years and reflect the marine reservoir age (Graham et al., 2017). However, this value probably does not reflect the local reservoir age in Little Jason Lagoon. Carbonates in 105 and 264 cm core depth gave ^{14}C ages of 1055±45 and 1180±40 yrs BP, respectively. A reservoir correction of 1100 years would imply unreasonably high sedimentation rates for the upper 260 cm of the sequence. The reservoir age in Little Jason Lagoon is likely lower than in the open marine setting and more likely reflected by the 720 years obtained from the recent, shallow water carbonate shell (Table 1). The modern carbonate shell can be affected by elevated ^{14}C concentration due to its post-bomb origin, which leads to an underestimation of the pre-bomb reservoir age. Gordon and Harkness (1992) suggested a pre-bomb reservoir correction of c. 750 years for South Georgia, which is in accordance with our findings. The difference in reservoir ages in the benthic foraminifers and the littoral carbonate could be due to the different carbon sources related to different water masses. Temperature and salinity profiles from Cumberland Bay indicate that the upper 25 metres of the water column are influenced by local melt water, while Antarctic Surface Water and Circumpolar Deep Water fill the deeper parts of the fjord (Geprägs et al., 2016). To account for the local reservoir effect we use a constant reservoir correction of 720 years for marine samples. It is highly likely that the reservoir age changed through time. Variable fresh-water run off, relative sea-level change, or changes in ocean circulation throughout the record may have changed the reservoir age. The quantification of such changes is not possible based on the data available and leads to some uncertainty in the age determination of the sediments and the in the age-depth model. For the establishment of an age depth-model terrestrial samples were calibrated with the SHcal13 dataset (Hogg et al., 2013) and samples of marine origin were calibrated with the Marine13 dataset (Reimer et al., 2013) using a reservoir correction of 720 years (ΔR=320 yrs). The age-depth model of core Co1305 was developed with the software Clam 2.2 (Blaaw, 2010) by a third order polynomial regression (Fig 6B).

DISCUSSION

Late Pleistocene de-glaciation (>11.2 ka)

The till recovered in Co1305 shows that the Little Jason Lagoon was glaciated. The occurrence of vascular plant *n*-alkanes in the lake sediments above the till points to the presence of catchment vegetation from the beginning of lake sedimentation. The soils surrounding Little Jason Lagoon therefore had stabilised by that time, which is also suggested by the diatom D. *stelligera*, which is typically not found in lakes immediately after local deglaciation and becomes abundant only once there is enough N and light available (Perren et al., 2017).

The glacial sediments in Little Jason Lagoon could correspond to an ice cap that covered Lewin Peninsula and had retreated from lower elevations around 16±1.5 ka (“stage 1-2”, Clapperton et al., 1989, White et al. 2017). However, the lake record indicates that some terrestrial vegetation already became established with the onset of lake sedimentation. Thus, we interpret unit I as a till produced by a local glacier flowing out of the Little Jason Lagoon catchment toward Jason Harbour from Jason Peak, which is consistent with the “stage 3” (Clapperton et al., 1989) moraine ridges around Little Jason Lagoon that post-date an ice cap retreat and document an expansion of local mountain glaciers down to modern sea level (White et al., 2017). The plants may have survived a late glacial advance (“stage 3”) in areas unaffected by glacier overriding and thus could disperse rapidly after glaciers retreated. This could explain the occurrence of terrestrial OM in the lake shortly after local glacier retreat. The relative sea level (RSL) was several metres below the present prior to 12 ka (Barlow et al., 2016) and land areas were exposed that are now below sea level. On these grounds land plants could have grown at the same time as glaciers terminated close to present sea level.

Based on the radiocarbon age of 14,870-15,370 cal yr BP of moss fragments, which were found in 1034 cm depth in unit II (COL2842, Table 1, Fig. 7E) this glacier advance can be tentatively correlated to the ACR time slice, when tide water glaciers re-advanced in Cumberland East Bay (15.2±0.3 to 13.3±0.15 ka, Graham et al., 2017; Fig. 7N), and perhaps also in Stromness Harbour (13.5±1.5 ka, Bentley et al., 2007, recalculated to Borchers et al., 2016 production rate; Fig. 7J). The ACR has been identified in marine and ice core records from Antarctica (Mulvaney et al., 2012; Xiao et al., 2016; Fig. 7P and 7R) and was associated with glacier advances in southern South America (e.g. Menounos et al., 2013). The record from South Georgia confirms the regional significance of this cooling event and supports previous findings of a strong impact of the ACR on the South Atlantic region (Pedro et al., 2016).

Early Holocene thermal maximum and relative sea level rise (< 11.2 to 7.0 ka)

The onset of lacustrine conditions in Little Jason Lagoon (unit II) indicates that de-glaciation of the area was sufficiently progressed to allow biogenic production in the lake. Subsequent decrease in the proportion of siliciclastic matter (increase in Si/Ti-ratio) likely before 11,120-11,245 cal yr BP (COL2210, Table 1) and an increase in OM in the sediments points to recession of glaciers in the catchment of the lake. Glacier retreat, lake productivity and increasing vegetation in and around Little Jason Lagoon were likely promoted by relatively mild conditions in the early Holocene. Marine records from the Atlantic sector of the Southern Ocean show that sea surface temperatures around South Georgia were close to modern values between 11 and 9 ka (e.g., Xiao et al., 2016; Fig. 7P). The relatively high temperatures likely affected environmental conditions on South Georgia and supported increasing vegetation and lake productivity in low altitude areas of South Georgia (e.g., Van der Putten et al., 2009, Hodgson et al., 2014b; Fig. 7N).

Aside from clearly dilute, oligotrophic taxa, 34 to 44% of the diatoms in unit II have broader salinity ranges (Fig. 3I), thereby suggesting that the lake was coastal in character and may have been occasionally affected by storm surges or salt spray. At 8.0±0.8 ka the record from Little Jason Lagoon shows a transition from fresh to marine conditions (unit II/unit III). In the beginning high contributions of brackish/benthic species suggests that the basin had not transitioned to full marine conditions. Episodes of high melt-water input or isolation from marine waters possibly have freshened waters sufficiently for brackish/benthic species to out-compete marine taxa. During the transgression, erosion of vegetation and soil from low-lying areas probably increased the input of plant material into Little Jason Lagoon as indicated by a distinct maximum in plant-derived *n*-alkane fluxes. Higher CPI values than in the underlying lacustrine sediments suggests that the material was relatively well preserved and likely derived from the input of plant material rather than degraded peats and soils. After the transition the flux of plant material and organic carbon contents in Little Jason Lagoon remained high until c. 7.0 ka. This points to extensive vegetation in the catchment and increased productivity in the marine inlet.

The transition from lacustrine to marine conditions resulted from a rise in relative sea level, as postglacial eustatic sea level rise outpaced glacio-isostatic uplift in South Georgia (Barlow et al., 2016). The diatom record shows that, after the transition, Little Jason Lagoon remained in contact with marine waters in Cumberland Bay until the present day. The persistence of marine conditions shows that Holocene glacier advances in Cumberland Bay West were not extensive enough to block off Jason Harbour. This supports previous findings, which assign an undated, partially-preserved outer moraine off Little Jason Lagoon to the older Antarctic cold reversal re-advance identified in Cumberland East Bay (Hodgson et al., 2014a; Graham et al., 2017).

Mid-Holocene glacier advance (7.0 to 4.0 ka)

Beginning at 7.0±0.6 ka lower Si/Ti-ratios reflect increasing input of siliclastic matter into Little Jason Lagoon (Fig. 7A). At the same time C concentrations decrease (Fig. 7B), which is likely an effect of dilution of the biogenic signal by higher proportions of siliciclastic matter. The input of land plant material decreased, pointing to reduced vegetation coverage of the terrestrial catchment (Fig. 7D). The increase in detrital input and a decrease in vegetation are best explained by the growth of glaciers in the catchment. Periglacial conditions in the proximity of the inlet led to higher input of siliciclastic material by meltwater runoff and mass movement processes and led to unstable grounds thereby reducing the vegetation coverage. Marine production decreased during this period, which is indicated by lowest $\delta^{13}C$ values of organic carbon in unit IV (Fig. 7C). This likely was an effect of high freshwater run-off from the local cirque glaciers, which is also indicated by the diatom assemblage in unit IV that reflects seasonal freshening of the upper water column. However, the prevailing marine conditions and production argue against an advance of local cirque glaciers down to sea level. Their maximum extent likely was down to c. 30 m a.s.l. as indicated by glacial deposits in the terrestrial catchment of Little Jason Lagoon, which have been assigned as “stage 4” deposits (White et al., 2017; Fig. 2B). In Little Jason Lagoon the increase in OM and land plant material after 5.3±0.5 ka points to a gradual reduction of glacier activity in the catchment. High Si/Ti ratios and high C contents at 4.0±0.4 ka indicate that glacier activity in the drainage basin of Little Jason Lagoon ceased.

Parallel to the increase in silicilastic matter Little Jason Lagoon received an increase in IRD influx (Fig. 7C). Since the cirque glaciers were likely not in direct contact with the inlet, IRD was not derived from calving of these glaciers. IRD input into Little Jason Lagoon could have occurred via sea ice, which is not supported by the diatoms that do not show significant changes in sea ice coverage throughout unit IV. As such, the IRD likely derived from a source external to the basin. At present icebergs originating from tidewater glaciers like Neumeyer Glacier are floating in Cumberland West Bay (Fig. 2A and B). The increase in IRD in Little Jason Lagoon starting around 7.0±0.6 ka possibly reflects higher input of small icebergs from the fjord. Higher RSL than at present (Barlow et al., 2016) likely provided better access of floating glacier ice to the inlet. The increased flux in icebergs could result from glaciers advancing into the fjord. Advance of some glaciers, which are presently not in contact with marine waters in Cumberland West Bay (Fig. 2A), are a likely source of IRD. Lateral moraines in Cumberland bays and Moraine Fjord indicate an advance that was in an order of several kilometres (Bentley et al., 2007). The retreat was dated to 3.6±1.1 ka BP (Bentley et al., 2007, Fig. 7I), which is consistent with decreasing IRD deposition in Little Jason Lagoon.

Glacier advances in South Georgia starting around 7.0±0.6 ka likely occurred against a background of cooling. This is not only suggested by a lowering of the equilibrium line altitude (ELA) of small mountain glaciers in South Georgia (White et al., 2017; Oppedal et al., 2018; 7H) but also by two peat sequences from Stromness Bay area. There high proportions of *Warnstorfia* spp. moss remains between c. 8 and 4.4 ka in indicate generally wet and possibly also cooler conditions (Van der Putten et al., 2009, Fig. 7N). Summer sea-surface temperatures in the Atlantic sector south of the Polar Front were below modern values during that time and the winter sea-ice edge likely reached the latitude of South Georgia (Xiao et al., 2016). Cooling of the surface waters in the Atlantic sector south of the Polar Front around 8 ka (Xiao et al., 2016, Fig. 7P) may have fostered cooling and growth of glaciers in South Georgia.

The timing of glacier advances in South Georgia is also in accordance with the Southern Patagonian Icefield, were the most extensive Holocene glacier coverage occurred during the interval from 6.1 to 4.5 ka (Kaplan et al., 2016, Fig. 7Q) and also consistent with the formation of moraines by extended cirque glaciers in southernmost Tierra del Fuego between 7.96-7.34 and 5.29-5.05 ka (Menousnos et al., 2013). In Southern Patagonia ice accumulation was promoted by colder air over the latitudes from 50 to 55°S, which may have resulted from a more equatorward position of the westerly winds (Kaplan et al., 2016). In the Antarctic Peninsula Region atmospheric cooling relative to the early Holocene occurred after c. 9 ka (Mulvaney et al., 2012, Fig. 7S). However, temperatures were not below modern values during the mid-Holocene. Mid-Holocene glacier and ice sheet advances from the Antarctic Peninsula region are not well constraint due to a scarcity of records and uncertainties in age determination (Ó Cofaigh et al., 2014).

Mid-Holocene warming (c. 4.0 to 1.8 ka)

After 4.0±0.4 ka sedimentation of OM was high in Little Jason Lagoon (high C contents; Fig. 7B). Small or no glaciers in the catchment and more retreated glaciers in the fjord likely promoted marine productivity by low siliciclastic input (high Si/Ti ratios, low/no IRD Fig. 7A and D). In contrast to total OM, the input of land plants into the marine inlet only gradually increased after glaciers retreated in the catchment (Fig. 7E). This likely reflects a delayed recovery of the local terrestrial vegetation due to re-colonisation of unstable, previously periglacial grounds and subsequent soil development. An increase of IRD supply around 3 ka could reflect increased calving of the fjord glaciers.

The dispersal of vegetation cover was probably supported by warmer conditions as indicated by a GDGT-derived temperature record from Fan Lake, Annenkov Island (Foster et al., 2016; Fig. 7P). Warmer and drier conditions between 4.4 and 3.0 ka were also reconstructed from plant macro fossil and pollen records from Stromness Bay and Annenkov Island, respectively (van der Putten et al., 2009; Strother et al., 2015, 7O). Land based glaciers were in more retreated positions after 4 ka (Strother et al., 2015, Barlow et al., 2016) and fjord glaciers were likely also less extensive. In Moraine Fjord soils and peat deposits formed between 3.5 and 2.0 ka, when the Nordenskjöld Glacier was in a more retreated position (Gordon, 1987; Clapperton et al., 1989, Fig. 7K).

Timing coincides with warmer conditions and glacier retreats on the Antarctic Peninsula and the South Shetland Islands, which were reconstructed for the period 4.5 to 2.8 ka (Hall, 2007; Bentley et al., 2009).

Late Holocene (c. 1.8 ka to present)

At 1.8 ± 0.3 ka a sharp drop in the Si/Ti ratio indicates a shift in sediment composition indicating the recurrence of glaciers in the catchment of the inlet (Fig 7A). In contrast to the mid-Holocene, the increase in siliciclastic input (low Si/Ti ratio) does not go along with reduced OM deposition as C contents remain high (Fig 7A and B). This could have resulted from constant autochthonous OM production as indicated by constant $\delta^{13}C$ values despite an increase in siliciclastic matter supply (Fig. 7C). OM preservation in the sediment was likely supported by rapid burial during high sedimentation rates (Fig. 6B). A drop in the input of land plant derived material around 0.7 ka did not occur synchronously with the beginning of the glacier advance suggested by the Si/Ti ratio (Fig 7E). The formation of glaciers possibly led to initially high fluxes of terrestrial OM into the inlet due to increased erosion in the catchment by meltwater run-off and slope instability. As a consequence vegetation density in the surroundings of the inlet was reduced which led to lower fluxes after 0.7 ka (Fig. 7E). The effect on the vegetation in the direct vicinity of Little Jason Lagoon as well as on the marine productivity was less pronounced than during the mid-Holocene. This indicates smaller glaciers and less severe change in environmental conditions than during the “neoglacial”. This supports previous studies which showed that late Holocene mountain glaciers on Lewin Peninsula were restricted to altitudes above 250 m a.s.l. (“stage 5” moraines; White et al., 2017; Figs. 2 and 7H). The temporal variability in Si/Ti ratios and variable land plant input into Little Jason Lagoon suggest subsequent fluctuations in glacier extent. However, a correlation with centennial-scale fluctuations such as the Little Ice Age (LIA) reported by van der Bilt et al. (2017; Fig. 7L) is hampered by the uncertainty in the age model-depth of our record. IRD sedimentation in Little Jason Lagoon increased around 1.8 ± 0.3 ka and attained highest values in the past c. 300 years (Fig. 7D). This indicates that not only the terrestrial catchment of the inlet was affected, but also iceberg calving in Cumberland Bay West increased, possibly due to expanded glaciers in the fjord. In Cumberland East Bay an advance of the Nordenskjöld Glacier commenced at 2.0 ka (Gordon, 1987; Clapperton et al., 1989, Fig 7K) and the glacier showed some subsequent fluctuations (Graham et al., 2017 Fig 7N). Glaciers in the terrestrial catchment of Little Jason Lagoon persisted until recently. Radiocarbon dated mosses indicate a shift from clastic to biogenic sedimentation in Jason Lake B located down slope of “stage 5” deposits around 0.46 ka (White et al., 2017, Figs. 2B and 7K), which likely reflects the end of glacier retreat. Since the organic matter formed in the lake could be affected by a reservoir age of up to several hundred years (Moreton et al., 2004), this date gives a maximum age.

Glacier advances in South Georgia during the late Holocene went along with cooling as suggested by GDGT-based (air) temperature reconstructions from Fan Lake, Annenkov Island (Foster et al., 2016, Fig. 7P). Plant communities in a peat sequence from Lewin Peninsula reflect a shift to wetter and/or colder conditions around 2.2 ka (Van der Putten et al., 2012, Fig 7O). Cooling was accompanied by strengthening of the westerly winds around 2.2 to 1.7 ka (Strother et al., 2015; Turney et al., 2016). It may also reflect a latitudinal displacement of the westerlies, which likely would have strong impact on South Georgia´s glaciers by altering precipitation rates (Sime et al., 2013).

A late Holocene atmospheric cooling starting after 2.5 ka was also recorded in an ice core from James Ross Island, Antarctic Peninsula (Mulvaney et al., 2012; Fig. 7R) and coincided with glacier advances in that region (Hall 2009; Bentley et al., 2009; Simms et al., 2012). Glacier advances also occurred in southern South America (e.g., Menounos et al., 2013; Kaplan et al. 2016; Fig. 7Q). In the more northern Patagonian Ice Field cirque glaciers were less advanced in the late Holocene than during the “neoglacial” (Kaplan et al., 2016), which is similar to the pattern we find in South Georgia, while in southernmost Tierra del Fuego LIA glacier limits are close to mid-Holocene limits or mark the most extensive Holocene glaciers

(Menounos et al., 2013).

SUMMARY AND CONCLUSIONS

Here we present a multi-proxy study of an 11.04 m long sediment core (Co1305) from a coastal inlet (Little Jason Lagoon). The local changes we identified in the sediment record reflect Late Quaternary changes in environmental conditions in South Georgia. Age determination of the sediments was achieved by ^{14}C analysis. We found that ^{14}C ages of bulk organic carbon are strongly biased by re-deposited and relict OM and do not reflect sedimentation age. In the scarcity of terrestrial macro fossils age control was obtained by compound-specific radiocarbon dating of mostly marine derived n-C_{16} fatty acids.

A basal till layer recovered in Little Jason Lagoon likely correlates with an advance of local glaciers during the Antarctic cold reversal. After glacier retreat an oligotrophic lake occupied the site. Diatom assemblage data, $\delta^{13}C$ values of organic carbon and C/N ratios show a transition into a marine inlet around 8.0±0.9 ka due to relative sea level rise. Reduced vegetation coverage in the catchment as well as high siliciclastic input and deposition of IRD point to glaciers advancing in the terrestrial catchment and likely in Cumberland West Bay from 7.0±0.6 to 4.0±0.4 ka. Our record provides new constraints on the timing of the "neoglacial" ice advance in South Georgia, in particular on the onset of glacier advances, which were not well constrained. A second, less extensive period of glacier advances occurred in the late Holocene, after 1.8 ± 0.3 ka. Our record suggests some fluctuation in glacier extent during this period, however, dating uncertainty of the marine sediments hampers correlation with centennial scale glacier fluctuations as reported from records in the region. Of particular value is the information obtained on the glacial history of the region, since it provides (i) tie points for the relative sea level history, which is directly linked to glaciation, (ii) a continuous record, as opposed to the discontinuous information derived from the investigation of moraines in the catchment, and (iii) an improved picture of the temporal development of land-based glaciers on South Georgia, which is complementary to geomorphological studies.

Our results confirm the region-wide nature of these millennial-scale events identified on South Georgia. We suggest that glacier advances on South Georgia during the Antarctic cold reversal were not restricted to the marine-terminating larger glacier systems in the fjords but also occurred at lower altitude mountain glaciers. This confirms that climate conditions in the latitude of South Georgia responded in concert with an Antarctic-wide cooling around 14.7 to 13 ka. The timing of a mid-Holocene “neoglacial” glacier advances on South Georgia between 7.0±0.6 and 4.0±0.4 ka correlates with a period of larger glaciers at the Southern Patagonian Icefield and southernmost Tierra del Fuego in South America, while evidence for glacier and ice sheet advances in the Antarctic Peninsula region are less clear. However, the timing of terrestrial glacier retreat in in the sub-Antarctic latitudes of the Atlantic sector of the Southern Ocean is broadly consistent with the onset of warmer conditions at the Antarctic Peninsula. Late Holocene glacier advances and regional cooling after c. 1.8 ± 0.3 ka is consistent with records from southern South America, Antarctic Peninsula and the sub-Antarctic. Air temperatures on the eastern side of the Antarctic Peninsula were lower in the past c. 2.5 kyrs than during the remainder of the Holocene and in southernmost South America late Holocene glaciers close to or beyond mid-Holocene limits. This differs from the glacier extent observed in South Georgia and in the more northern parts of southern South America where late Holocene glacier advances were less extensive than during the mid-Holocene.

Comparing the pattern of Holocene millennial-scale glacier behaviour in South Georgia to glacier advances and retreats in southern Patagonia as well as in the Antarctic Peninsula region shows some similarities in timing, however correlations in the magnitude of glacier advances north and south differ over time. This reflects that South Georgia is a key area for investigating the teleconnections of climate changes between Antarctica and lower latitudes.

ACKNOWLEDGEMENTS

This work was supported by the Deutsche Forschungsgemeinschaft (DFG) in the framework of the priority program “Antarctic Research with comparative investigations in Arctic ice areas” by grant BE 4764/3-1. Additional funding was provided to SB by a University of Cologne (UoC) Postdoc grant. Furthermore, DW and SB have been supported by grants from the Universities Australia-DAAD Joint Research Cooperation Scheme (Project: Past Environmental Changes in the Sub-Antarctic). Ulrike Patt, Volker Wennrich and Sonja Groten are thanked for assistance in the lab and Benedikt Ritter for assistance in field. The fieldwork was carried out within the scope of the RV *Polarstern* cruise ANT XXIX/4; we are grateful to the captain, the crew and in particular the cruise leader Gerhard Bohrmann for various support. We also like to thank the Government of South Georgia and the South Sandwich Islands for providing helpful advises and the permission for fieldwork. The manuscript strongly benefited from comments of Dominic A. Hodgson and two anonymous reviewers.

REFERENCES

Al-Handal, A.Y., Wulff, A., 2008a. Marine benthic diatoms from Potter Cove, King George Island, Antarctica. Botanica Marina 51, 51-68.

Al-Handal, A.Y., Wulff, A., 2008b. Marine epiphytic diatoms from the shallow sublittoral zone in Potter Cove, King George Island, Antarctica. Botanica Marina 51, 411-435.

Andersson, R.A., Meyers, P.A., 2012. Effect of climate change on the delivery and degradation of lipid biomarkers in a Holocene peat sequence in the Eastern European Russian Arctic. Organic Geochemistry 53, 63-72.

Angst, G., John, S., Mueller, C.W., Kögel-Knabner, I., Rethemeyer, J., 2016. Tracing the sources and spatial distribution of organic carbon in subsoils using a multi-biomarker approach. Scientific Reports 6, Arcticle number 29478.

Barlow, N.L.M., Bentley, M.J., Spada, G., Evans, D.J., Hansom, J.D., Brader, M.D., White, D.A., Zander, A., Berg, S., 2016. Testing models of ice cap extent, South Georgia, sub-Antarctic. Quaternary Science Reviews 154, 157-168.

Bentley, M.J., Evans, D.J.A., Fogwill, C.J., Hansom, J.D., Sugden, D.E., Kubik, P.W., 2007. Glacial geomorphology and chronology of deglaciation, South Georgia, sub-Antarctic. Quaternary Science Reviews 26, 644–677.

Bentley, M.J., Hodgson, D.A., Smith, J.A., O'Cofaigh, C., Domack, E.W., Larter, R.D., Roberts, S.J., Brachfeld, S., Leventer, A., Hjort, C., Hillenbrand, C.D., Evans, J., 2009. Mechanisms of Holocene palaeoenvironmental change in the Antarctic Peninsula region. The Holocene 19, 51–69.

Blaaw M., 2010. Methods and code for 'classical' age-modelling of radiocarbon sequences. Quaternary Geochronology 5, 512–518.

Borchers, B., Marrero, S., Balco, G., Caffee, M., Goehring, B., Lifton, N., Nishiizumi, K., Phillips, F., Schaefer, J., Stone, J., 2016. Geochronological calibration of spallation production rates in the CRONUS-Earth project. Quaternary Geochronology 31, 188-198.

Croudace, I.W., Rindby, A., Rothwell, R.G., 2006. ITRAX: description and evaluation of a new multi-function X-ray core scanner. In: Rothwell, R.G. (ed.) New techniques in sediment core analysis. Geological Society, London, Special Publications 267, 51-63.

Clapperton, C.M., Sugden, D.E., Birnie, J., Wilson, M.J., 1989. Late-glacial and Holocene glacier fluctuations and environmental change on South Georgia, Southern Ocean. Quaternary Research 31, 210-228.

Clapperton, C.M., 1990. Quaternary glaciations in the Southern Ocean and Antarctic Peninsula area. Quaternary Science Reviews 9, 229-252.

Dewald, A., Heinze, S., Jolie, J., Zilges, A., Dunai, T., Rethemeyer, J., Melles, M., Staubwasser, M., Kuczewski, B., Richter, J., Radtke, U., von Blanckenburg, F., Klein, M., 2013. CologneAMS, a dedicated centre for accelerator mass spectrometry in

Germany. Nuclear Instruments Methods Phys. Res. Sect. B Beam Interact. Mater. Atoms 294, 18–23.

Drenzek, N.J., Montucon, D.B., Yunker, M.B., Macdonald, R.W., Eglinton, T.I. 2007. Constraints on the origin of sedimentary organic carbon in the Beaufort Sea from coupled molecular ^{13}C and ^{14}C measurements. Marine Chemistry 103, 146-162.

Eglinton, G., Hamilton, R.J., 1963. The distribution of Alkanes. In: Swain, T. (Ed.) Chemical Plant Taxonomy. Academic Press Inc. 187- 217.

Eyles, N., Mullins, H.T., Hine, A.C. 1991. The seismic stratigraphy of Okanagan Lake, British Columbia; a record of rapid deglaciation in a deep „fjord-lake“ basin. Sedimentary Geology 73, 13-41.

Favier, V., Verfaillie, D., Berthier, E., Menegoz, M., Jomelli, V., Kay, J.E., Ducret, L., Malbéteau, Y., Brunstein, D., Gallée, H., Park, Y.H., Rinterknecht, V. 2016. Atmospheric drying as the main driver of dramatic glacier wastage in the southern Indian Ocean. Scientific Reports 6, 32396

Foster, L.C., Pearson, E.J., Juggins, S., Hodgson, D.A., Saunders, K.M., Verleyen, E., Roberts, S.J., 2016. Development of a regional glycerol dialkyl glycol tetraether (GDGT) - temperature calibration for Antarctic and sub-Antarctic lakes. Earth and Planetary Science Letters 433, 370-379.

Geprägs P., Torres, M.E., Mau, S., Kasten, S., Römer, M., Bohrmann, G., 2016. Carbon cycling fed by methane seepage at the shallow Cumberland Bay, South Georgia, sub-Antarctic. Geochemistry, Geophysics, Geosystems, doi 10.1002/2016GC6276.

Gordon, J.E., 1987. Radiocarbon dates from the Nordenskjöld Glacier, South Georgia, and their implications for late Holocene glacier chronology. British Antarctic Survey Bulletin 76, 1-5.

Gordon, J.E., Harkness D.D., 1992. Magnitude and geographic variation of the radiocarbon content in Antarctic marine life: Implications for reservoir corrections in radiocarbon dating. Quaternary Science Reviews 11, 697-708.

Gordon, J.E., Timmis, R.J., 1992. Glacier fluctuations on South Georgia during the 1970s and early 1980s. Antarctic Science 4, 215-226.

Gordon, J.E., Haynes, V.M., Hubbard, A., 2008. Recent glacier changes and climate trends on South Georgia. Global and Planetary Change 60, 72-84.

Graham, A.G.C., Fretwell, P.T., Larter, R.D., Hodgson, D.A., Wilson, C.K., Tate, A.J., Morris, P., 2008. A new bathymetric compilation highlighting extensive paleo–ice sheet drainage on the continental shelf, South Georgia, sub-Antarctica. Geochemistry, Geophysics, Geosystems 9, 1-21.

Graham, A.G.C., Kuhn, G., Meisel, O., Hillenbrand, C.-D., Hodgson, D.A., Ehrmann, W., Wacker, L., Wintersteller, P., dos Santos Ferreira, C., Römer, M., White, D., Bohrmann, G., 2017. Major advance of South Georgia glaciers during the Antarctic Cold Reversal following extensive sub-Antarctic glaciation. Nature Communications doi: 10.1038/ncomms14798.

Greene, S.W., 1964. The vascular flora of South Georgia. British Antarctic Survey, Scientific Reports 45, 58 pp.

Grobe, H., 1987. A simple method for the determination of ice-rafted debris in sediment cores. Polarforschung 57, 123-126.

Hall, B., 2009. Holocene glacial history of Antarctica and the sub-Antarctic islands. Quaternary Science Reviews 28, 2213-2230.

Hargraves, P.E., French, F.W., 1983. Diatom resting spores: Significance and strategies. In: Fryxell, G., Survival Strategies of the Algae. Cambridge University Press, New York, pp. 49-68.

Hasle, G.R., Syvertsen, E.E., 1997. Chapter 2: Marine Diatoms. In: Tomas, C.R. (Ed.) Identifying Marine Phytoplankton. Academic Press, San Diego, pp. 5-385.

Hodgson, D.A., Graham, A.G.C., Giffiths, H.J., Roberts, S.J., Ó Cofaigh, C., Bentley, M.J., Evans, D.J.A., 2014a. Glacial history of sub-Antarctic South Georgia based on the submarine geomorphology of its fjords. Quaternary Science Reviews 89, 129-147.

Hodgson, D.A., Graham, A.G.C., Roberts, S.J., Bentley, M.J., Ó Cofaigh, C., Verleyen, E., Vyverman, W., Jomelli, V., Favier, V., Brunstein, D., Verfaillie, D., Colhoun, E.A., Saunders, K.M., Selkirk, P.M., Mackintosh, A., Hedding, D.W., Nel, W., Hall, K., McGlone, M.S., Van der Putten, N., Dickens, W.A., Smith, J.A., 2014b. Terrestrial and submarine evidence for the extent and timing of the Last Glacial Maximum and the onset of deglaciation on the maritime-Antarctic and sub-Antarctic islands. Quaternary Science Reviews 100, 137-158.

Hogg, A.G., Hua, Q., Blackwell, P.G., Buck, C.E., Guilderson, T.P., Heaton, T.J., Niu, M., Palmer, J.G., Reimer, P.J., Reimer, R.W., Turney, C.S.M., Zimmerman, S.R.H., 2013. Shcal13 southern hemisphere calibration, 0–50,000 years cal BP. Radiocarbon 55, 1889-1903.

Höfle, S., Rethemeyer, J., Mueller, C.W., John, S. 2013. Organic matter composition and stabilization in a polygonal tundra soil of the Lena Delta. Biogeosciences 10, 3145-3158.

Johansen, J.R., Fryxell, G.A., 1985. The genus Thalassiosira (Bacillariophyceae): studies on species occurring south of the Antarctic Convergence Zone. Phycologia 24, 155-179.

Kaplan, M.R., Schaefer, J.M., Strelin, J.A., Denton, G.H., Anderson, R.F., Vandergoes, M.J., Finkel, R.C., Schwartz, R., Travis, S.G., Garcia, J.L., Martini, M.A., Nielsen, S.H.H., 2016. Patagonian and southern South Atlantic view of Holocene climate. Quaternary Science Reviews 141, 112-125.

Krebs, W.N., 1983. Ecology of neritic marine diatoms, Arthur Harbor, Antarctica. 0026-2803 29, 267-297.

Lamb, A.L., Wilson, G.P., Leng, M.J., 2006. A review of coastal palaeoclimate and relative sea-level reconstructions using $\delta^{13}C$ and C/N ratios in organic material. Earth-Science Reviews 75, 29-57.

Lamy, F., Kilian, R., Arz, H.W., Francois, J.-P., Kaiser, J., Prange, M., Steinke, T., 2010. Holocene changes in the position and intensity of the southern westerly wind belt. Nature Geoscience 3, 695-699.

Lange, P., Tenenbaum, D., De Santis Braga, E., Campos, L., 2007. Microphytoplankton assemblages in shallow waters at Admiralty Bay (King George Island, Antarctica) during the summer 2002–2003. Polar Biology 30, 1483-1492.

Leng, M., Lewis, J.P., 2017. C/N ratios and carbon isotope composition of organic matter in estuarine environments. In: Weckström, K. Saunders, K. Gell, P. Skilbeck, G. (Eds.) Applications of Paleoenvironmental Techniques in Estuarine Studies, pp. 213-327.

Marzi, R., Torkelson, B.E., Olson, R.K., 1993. A revised carbon preference index. Organic Geochemistry 8, 1303-1306.

Melles, M., Bennicke, O., Leng, M., Ritter B., Viehberg, F., White, D., 2013. Late Quaternary climatic and environmental history of South Georgia. In: G. Bohrmann (Ed.) The Expedition of the Research Vessel "*Polarstern*" to the Antarctic in 2013 (ANT-XXIX/4). Reports on Polar and Marine Research 668, 117–135.

Menounos, B., Clague, J.J., Osborn, G., Davis, P.T., Ponce, F., Goehring, B., Maurer, M., Rabassa, J., Coronato, A., Marr, R., 2013. Latest Pleistocene and Holocene glacier fluctuations in southernmost Tierra del Fuego, Argentina. Quaternary Science Reviews 77, 70-79.

Moreton, S.G., Rosqvist, G.C., Davies, S.J., Bentley, M.J., 2004. Radiocarbon reservoir ages from freshwater lakes, South Georgia, sub-Antarctic: modern analogues from particulate organic matter and surface sediments. Radiocarbon 46, 621-662.

Mulvaney, R., Abram, N.J., Hindmarsh, R.C.A., Arrowsmith, C., Fleet, L., Triest, J., Sime, L.C., Alemany, O., Foord, S., 2012. Recent Antarctic Peninsula warming relative to Holocene climate and ice-shelf history. Nature 489, 141-145.

Ó Cofaigh, C., Davies, B., Livingstone, S.J., Smith, J., Johnson, J.S., Hocking, E.P., Hodgson, D.A., Anderson, J.B., Bentley, M.J., Canals, M., Domack, E., Dowdeswell, J.A., Evans, J., Glasser, N.F., Hillenbrand, C.D., Larter, R.D., Roberts, S.J., Simms, A.R. 2014. Reconstruction of ice-sheet changes in the Antarctic Peninsula since the Last Glacial Maximum. Quaternary Science Reviews 100, 87-110.

Oerlemans, J., 2005. Extracting a climate signal from 169 glacier records. Science 29, 675-677.

Ohkuchi, N., Eglinton, T.I., 2008. Compound-specific radiocarbon dating of Ross Sea sediments: A prospect for constructing chronologies in high-latitude oceanic sediments. Quaternary Geochronology 3, 235-243.

Oppedal, L.T., Bakke, J., Paasche, Ø., Werner, J.P., van der Bilt, W.G.M., 2018. Cirque glaciers on South Georgia shows centennial variability over the last 7000 years. Frontiers in Earth Science 6, doi: 10.3389/feart.2018.00002

Orsi, A.H., Witworth III, T., Nowlin, W.D., 1995. On the meridional extent and fronts of the Antarctic Circum Polar Current. Deep-Sea Research I 42, 641-673.

Pancost, R., Boot, C.S., 2004. The paleoclimatic utility of terrestrial biomarkers in marine sediments. Marine Chemistry 92, 239-261.

Pedro, J.B., Bostock, H.C., Bitz, C.M., He, F., Vandergoes, M.J., Steig, E.J., Chase, B.M, Krause, C.E., Rasmussen, S.O., Markle, B.R., Cortese, G., 2016. The spatial extent and dynamics of the Antarctic Cold Reversal. Nature Geoscience 9, 51-55.

Perren, B., Axford, Y., Kaufman, D.S., 2017. Alder, nitrogen, and lake ecology: Terrestrial-aquatic linkages in the postglacial history of Lone Spruce Pond, South-western Alaska. PLOS ONE 12, e0169106. https://doi.org/10.1371/journal.pone.0169106

Reimer, P., Bard, E., Bayliss, A., Beck, J.W., Blackwell, P.G., Bronk Ramsey, C., Buck, C.E., Cheng, H., Edwards, R.L., Friedrich, M., Grootes, P.M., Guilderson, T.P., Haflidason, H., Hajdas, I., Hatté, C., Heaton, T.J., Hoffmann, D.L., Hogg, A.G., Hughen, K.A., Kaiser, K.F., Kromer, B., Manning, S.W., Niu, M., Reimer, R.W., Richards, D.A., Scott, E.M., Southon, J.R., Staff, R.A., Turney, C.S.M., van der Plicht, J., 2013. INTCAL13 and Marine13 radiocarbon age calibration curves 0-50,000 years cal BP. Radiocarbon 55, 1869-1887.

Rethemeyer, J., Dewald, A., Fülöp, R., Hajdas, I., Höfle, S., Patt, U., Stapper, B., Wacker, L., 2013. Sample preparation facilities for ^{14}C analysis at the new CologneAMS centre. Nuclear Instruments and Methods in Physics Research B 294, 168-172.

Roberts, S.J., Hodgson, D.A., Shelley, S., Royles, J., Griffiths, H.J., Deen, T.J., Thorne, M.A.S., 2010. Establishing lichenometric ages for nineteenth- and twentieth-century glacier fluctuations on South Georgia (South Atlantic). Geografiska Annaler 92A, 125-139.

Rosqvist, G.C., Rietti-Shati, M., Shemesh, A., 1999. Late glacial to middle Holocene climate record of lacustrine biogenic silica oxygen isotopes from a Southern Ocean island. Geology 27, 967-970.

Rosqvist, G.C., Schuber, P., 2003. Millennial-scale climate changes on South Georgia, Southern Ocean. Quaternary Research 59, 470-475.

Sakamoto, T. Ikehara, M., Aoki, K., Iijima, K., Kimura, N., Nakatsuka, T., Wakatsuchi, M., 2005. Ice-rafted debris (IRD)-based sea-ice expansion events during the past 100kyrs in the Okhotsk Sea. Deep-Sea Research II 52, 2275-2301.

Saros, J.E., Anderson N.J., 2015. The ecology of the planktonic diatom *Cyclotella* and its implications for global environmental change studies. Biological Reviews 90, 522–541.

Scherer, R.P., 1994. A new method for the determination of absolute abundance of diatoms and other silt-sized sedimentary particles. Journal of Paleolimnology 12, 171-179.

Scott, F.J., Thomas, D.P., 2005. Diatoms. In: Scott, F.J., Marchant, H.J. (Eds.), Antarctic Marine Protists. Australian Biological Resources Study, Australian Antarctic Division, Canberra and Hobart, 13-201.

Sime, L.C., Kohfeld, K.E., Le Quéré, C., Wolff, E.W., de Boer, A.M., Graham, R.M., Bopp, L. 2013. Southern Hemisphere westerly wind changes during the Last Glacial Maximum: model-data comparison. Quaternary Science Reviews, 64, 104-120.

Simms, A.R., Ivins, E.R., DeWitt, R., Kouremenos, P., Simkins, L.M., 2012. Timing of the most recent Neoglacial advance and retreat in the South Shetland Islands, Antarctic Peninsula: insights from raised beaches and Holocene uplift rates. Quaternary Science Reviews 47, 41-55.

Smith, R.I., 2000. Diamictic sediments within high Arctic lake sediments cores: evidence for lake ice rafting along the lateral glacial margin. Sedimentology 47, 1157-1179.

Strother, S.L., Salzmann, U., Roberts, S.J., Hodgson, D.A., Woodward, J., Van Nieuvenhuyze, W., Verleyen, E., Vyverman, W., Moreton, S.G., 2015. Changes in

Holocene climate and the intensity of Southern Hemisphere Westerly Winds based on a high-resolution palynological record from sub-Antarctic South Georgia. The Holocene 25, 263–279.

Stuiver, M., Reimer, P.J., 1993. Radiocarbon 35, 215-230.

Toggweiler, J.R., 2009. Shifting Westerlies. Science 323, 1434-1435.

Trouet V., Van Oldenborgh G.J., 2013. KNMI Climate Explorer: a web-based research tool for high-resolution paleoclimatology. Tree-Ring Research 69, 3–13. Turney, C.S.M., Jones, R.T., Fogwill, C., Hatton, J., Williams, A.N., Hogg, A., Thomas, Z.A., Palmer, J., Mooney, S., Reimer, R.W., 2016. A 250-year periodicity in the Southern Hemisphere westerly winds over the last 2600 years. Climate of the Past 12, 189-200.

Uchida, M., Shibata, Y., Kawamura, K., Kumamoto, Y., Yoneda, M., Ohkushi, K., Harada, N., Hirota, M., Mukai, H., Tanaka, A., Kusakabe, M., Morita, M., 2001. Compound-specific radiocarbon ages of fatty acids in marine sediments from the Western North Pacific. Radiocarbon 43, 949-956.

Van der Bilt, W.G.M., Bakke, J., Werner, J.P., Paasche, O., Rosqvist, G., Solheim Vatle, S., 2017. Late Holocene glacier reconstructions reveals retreat behind present limits and two-stage Little Ice Age on subantarctic South Georgia. Journal of Quaternary Science DOI: 10.1002/jqs.2937

Van der Putten, N., Stieperaere, H., Verbruggen, C., Ochyra, R., 2004. Holocene palaeoecology and climate history of South Georgia (sub-Antarctica) based on a macrofossil record of bryophytes and seeds. The Holocene 14, 382-392.

Van der Putten, N., Verbruggen, C., 2005. The onset of deglaciation of Cumberland Bay and Stromness Bay, South Georgia. Antarcic Science 17, 29-32.

Van der Putten, N., Verbruggen, C., Ochyra, R., Spassov, S., de Beaulieu, J-L., De Dapper, M., Hus J., Thouveny, N., 2009. Peat bank growth, Holocene palaeoecology and climate history of South Georgia (sub-Antarctica), based on a botanical macrofossil record. Quaternary Science Reviews 28, 65-79.

Van der Putten, N., Verbruggen, C., Björck S., de Beaulieu, J.-L., Barrow, C.J., Frenot, Y.,

2012. Is palynology a credible climate proxy in the Subantarctic? The Holocene 22, 1113-1121.

Volkman, J. K., Johns, R. B., Gillan, F. T., Perry, G. J., Bavor, H. J. Jr., 1980. Microbial lipids of an intertidal sediment—I. Fatty acids and hydrocarbons. Geochimica et Cosmochimca Acta 44, 1133–1143.

Wacker, L., Bonani, G., Friedrich, M., Hajadas, I., Kromer, B., Nemec, M., Ruff, M., Suter, M., Synal, H.-A., Vockenhuber, C., 2010. MICADAS: routine and high-precision radiocarbon dating. Radiocarbon 52, 252-262.

White, D.A., Bennike, O., Melles, M., Berg, S., 2017. Was South Georgia covered by an ice cap during the Last Glacial Maximum? In: Siegert, M.J. Jamieson, S.S.R., White, D.A. (Eds.), Exploration of Subsurface Antarctica: Uncovering Past Changes and Modern Processes. Geological Society, London, Special Publications 461. doi.org/10.1144/SP461.4

Xiao, W., Esper, O., Gersonde, R., 2016. Last Glacial-Holocene climate variability in the Atlantic sector of the Southern Ocean. Quaternary Science Reviews 135, 115-137.

Tables

Table 1

Conventional ^{14}C ages obtained for bulk organic matter (OM), *n*-C_{16} fatty acids (FA), carbonates, and plant debris (kelp and mosses) from sediments of core Co1305. ^{14}C value of 720 years for a modern carbonate shell from Grytviken was used to estimate a marine reservoir correction. A constant value was used to correct samples of marine origin (carbonates, *n*-C_{16} FA and kelp) for a local reservoir effect (^{14}C age corr.). Age range of calibrated ages are given for samples, which are considered in our interpretation. Marine samples were calibrated with the dataset marine13 (ΔR=320 years, Reimer et al., 2013) and samples of terrestrial origin were calibrated with SHcal13 (Hogg et al., 2013).

Figures

Figure 1

Map of the southwestern Atlantic Ocean showing the locations of South Georgia and the bordering land masses of South America, the Antarctic Peninsula (James Ross Island (JRI) and South Shetland Islands (SSI)) and East Antarctica. Positions of the Southern Antarctic Circumpolar Current Front (SACCF), the Polar Front (PF), the sub-Antarctic Front (SAF), and the Subtropical Front (STF) after Orsi et al., 1995.

Figure 2

A: Overview map of the central part of South Georgia showing the modern perennial snow and ice cover and geographical terms mentioned in the text. B: Digital elevation model of the surroundings of Little Jason Lagoon (LJL) at the northern shore of Cumberland West Bay (for location see orange rectangle in (A)), with the coring location Co1305. Coloured lines indicate limits of glacier advances (stages 3 to 5,) according to White et al., (2017) and the locations of streams entering LJL today.

Figure 3

Lithology and proxy data of the core composite Co1305 versus sediment depth. Major lithological characteristics (A), radiocarbon ages [^{14}C yr BP] (B), ice-rafted debris (IRD) given as grains >1 mm per gram dry sediment (C), Ti counts [cps] and Si/Ti ratio (10 point running average) (D), C_{25} to C_{35} *n*-alkanes [µg per gram TOC] and proportion of leaf wax derived high molecular weight (HMW) *n*-alkanes C_{27},C_{29}, C_{31} [%] (E), total carbon (C) and total sulphur (S) content [%] (F), water content [%] (G), C/N ratio and $\delta^{13}C$ of organic carbon (H), proportions of fresh water (fresh), brackish/benthic (b/b) and marine diatom species (I), and lithological units (J).

Figure 4

$\delta^{13}C$ of organic carbon versus C/N ratio of the OM (measured on the same aliquot). The lithological units can be clearly distinguished by their $\delta^{13}C$ and C/N-signatures. Typical $\delta^{13}C$ and C/N ranges for organic inputs are given (after Lamb et al., 2006)

Figure 5

n-Alkane concentrations (C_{25} to C_{35}) of sediment samples from core Co1305 versus carbon preference index (CPI). CPI was calculated for chain lengths of C_{25} to C_{35} (CPI= (C_{25}+ C_{27}+ ... C_{33}) + (C_{27}+ C_{27}+ ... C_{35}) / 2*(C_{26}+ C_{28}+ ... C_{34}), Marzi et al., 1993). For reference CPI values of tussock grass and a terrestrial mosses sampled from the catchment of LJL are given as well as the range of CPI values of lake sediments from Holocene sediments of a lake on Lewin Peninsula.

Figure 6

Radiocarbon ages and age-depth model for core Co1305 A: Conventional ^{14}C ages (yr BP) from bulk OM, *n*-C_{16} FA, terrestrial (moss) and marine (kelp and carbonate) fossils shown versus depth. ^{14}C ages shown here are not corrected for reservoir age B: Age-depth model created by polynomial interpolation between neighbouring levels (Clam 2.2., Blaaw, 2010). The model is based on the *n*-C_{16} FA ages, carbonate and marine macro algae. Calibrated ages of plant remains provide maximum ages of deposition for unit II.

Figure 7

Summary of records from South Georgia (A to P) and beyond (Q to S) shown versus age. (A) Si/Ti ratio, (B) organic C content [wt%], (C) $\delta^{13}C$ values of the bulk OM, (D) IRD flux [grains* yr^{-1}*cm^{-2}], and (E) Flux of HMW *n*-alkanes (C_{25} to C_{35}) [µg* yr^{-1}*cm^{-2}] in core Co1305 from Little Jason Lagoon (F) Green stars indicate age range (calibrated ^{14}C ages) of moss fragments from core Co1305. (G) Depositional environment in Little Jason Lagoon. Interpretation is based on the lithology, the stable isotopes and diatom data. Underlain in grey are periods of increased glacier activity as reconstructed in this study (H) Equilibrium line altitudes (ELA) of glaciers advances “stage 3” to “stage 5” as identified on Lewin Peninsula (White et al., 2017). Timing of glacier advances is inferred from the Little Jason Lagoon record. (I to P) Age constraints of Holocene glacier advances on South Georgia from different archives, with (I) Infrared stimulated luminescence (IRSL) ages of dunes on raised beaches (Barlow et al., 2016), (J) exposure ages of moraine deposits (Bentley et al., 2007, White et al., 2017), (K) ^{14}C-ages of plant fossils collected in stratigraphic context of moraine formation (Clapperton et al., 1989, White et al., 2017), (L) lake sediments from Hamberg Lakes (van der Bilt et al., 2017) and (M) pro-glacial Block Lake (Rosqvist and Schuber 2003), (N) marine sediments from Cumberland Bay (Graham et al., 2017), (O) peat deposits from Tønsberg Peninsula (Van der Putten et al., 2004) and Lewin Peninsula (Van der Putten et al., 2009), and (P) Holocene temperatures derived from Fan Lake sediments on Annencov Island (Forster et al., 2016). (Q): Diatom-based summer sea surface temperatures from the Atlantic sector of the Southern Ocean, south of PF (Xiao et al., 2016). (R) Holocene glacier advances in southern South America at the Southern Patagonian Icefield, Lago Argentino

(Kaplan et al., 2016) (S) Air temperatures from ice core from James Ross Island, Antarctic Peninsula (Mulvaney et al., 2012); see Figs. 1 and 2 for location maps.

Figure 1

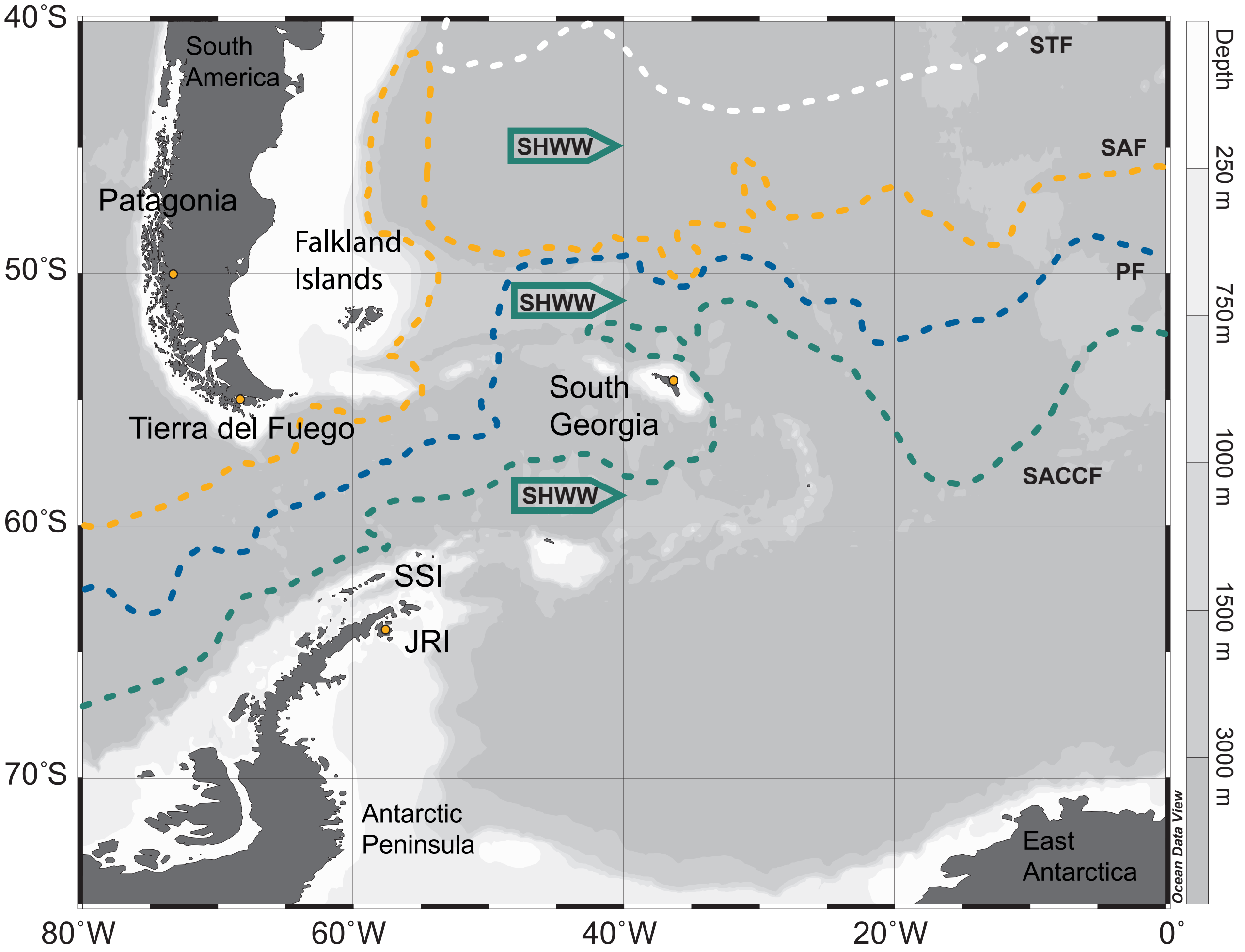
40°S
50°S
60°S
70°S
80°W
60°W
40°W
20°W
0°
South America
Patagonia
Falkland Islands
Tierra del Fuego
South Georgia
SSI
JRI
Antarctic Peninsula
East Antarctica
SHWW
SHWW
SHWW
STF
SAF
PF
SACCF
Depth
250 m
750 m
1000 m
1500 m
3000 m
Ocean Data View

Figure 2

Click here to download Figure Figure 2.pdf

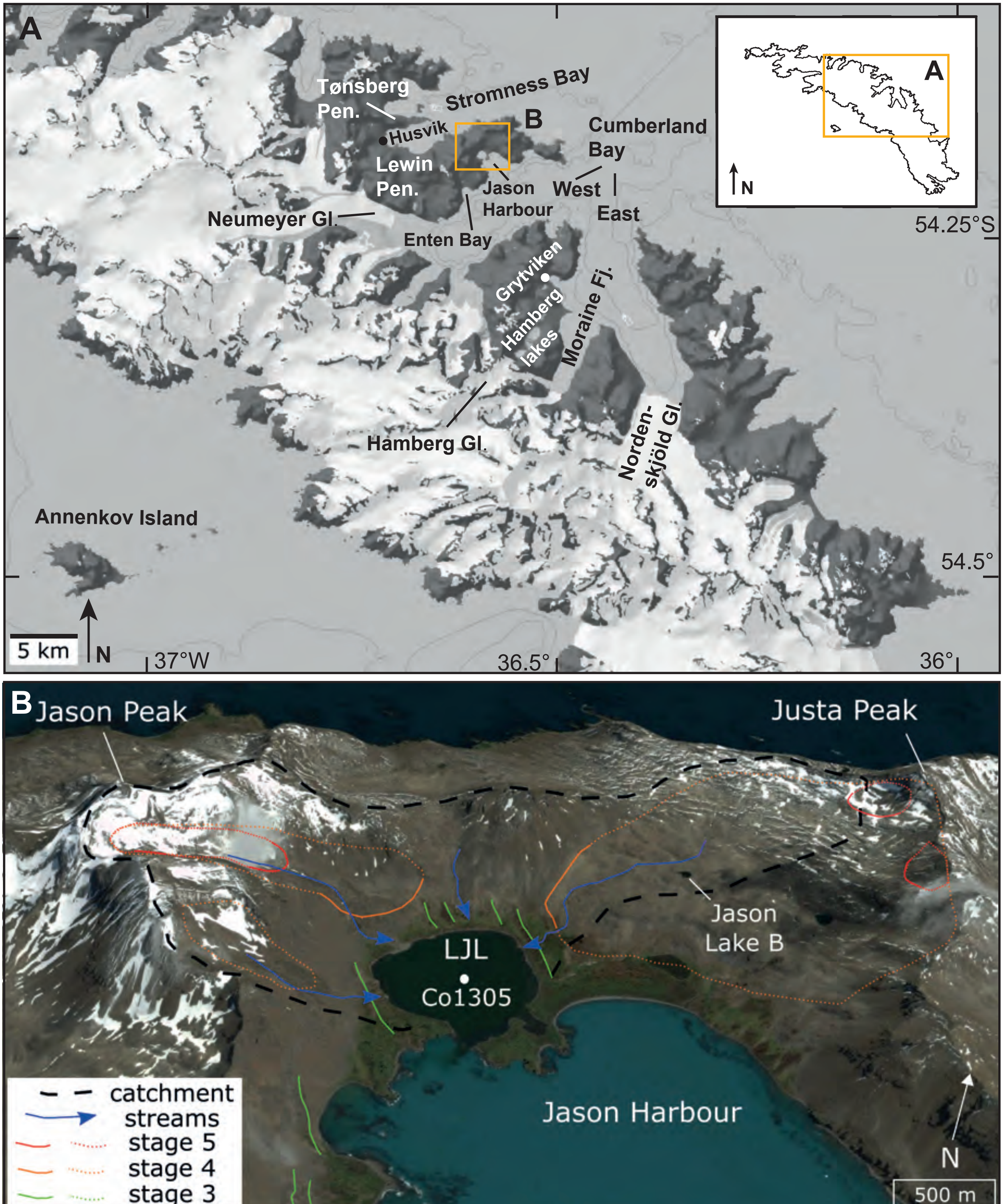

Figure 3

Click here to download Figure Figure 3.pdf

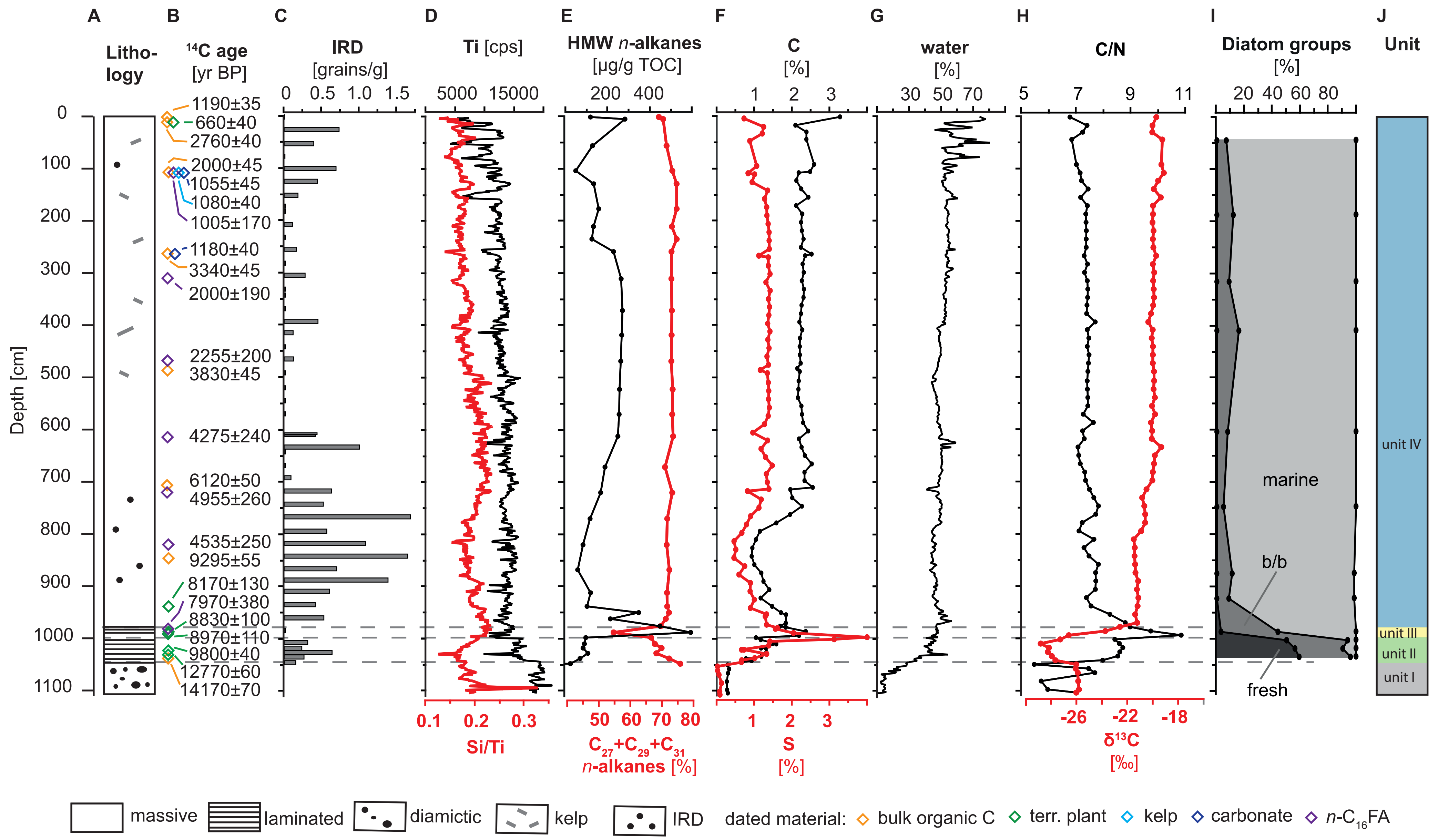

Figure 4

Click here to download Figure Figure 4.pdf

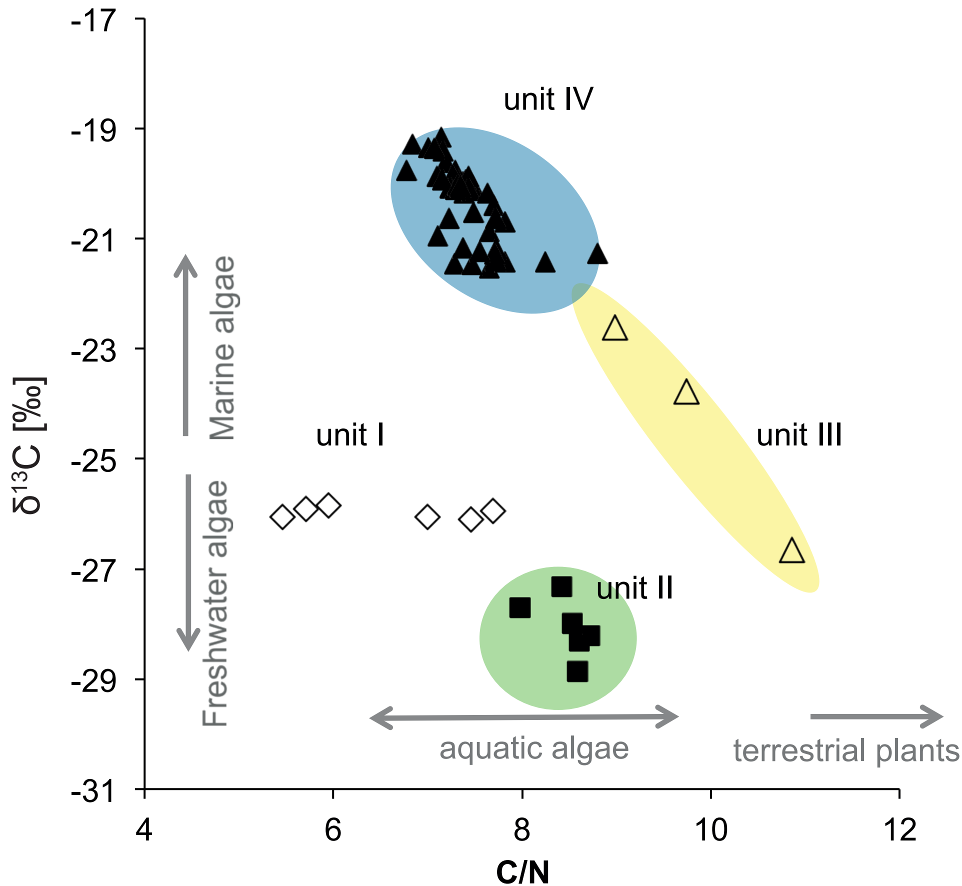

Figure 5

Click here to download Figure Figure 5.pdf

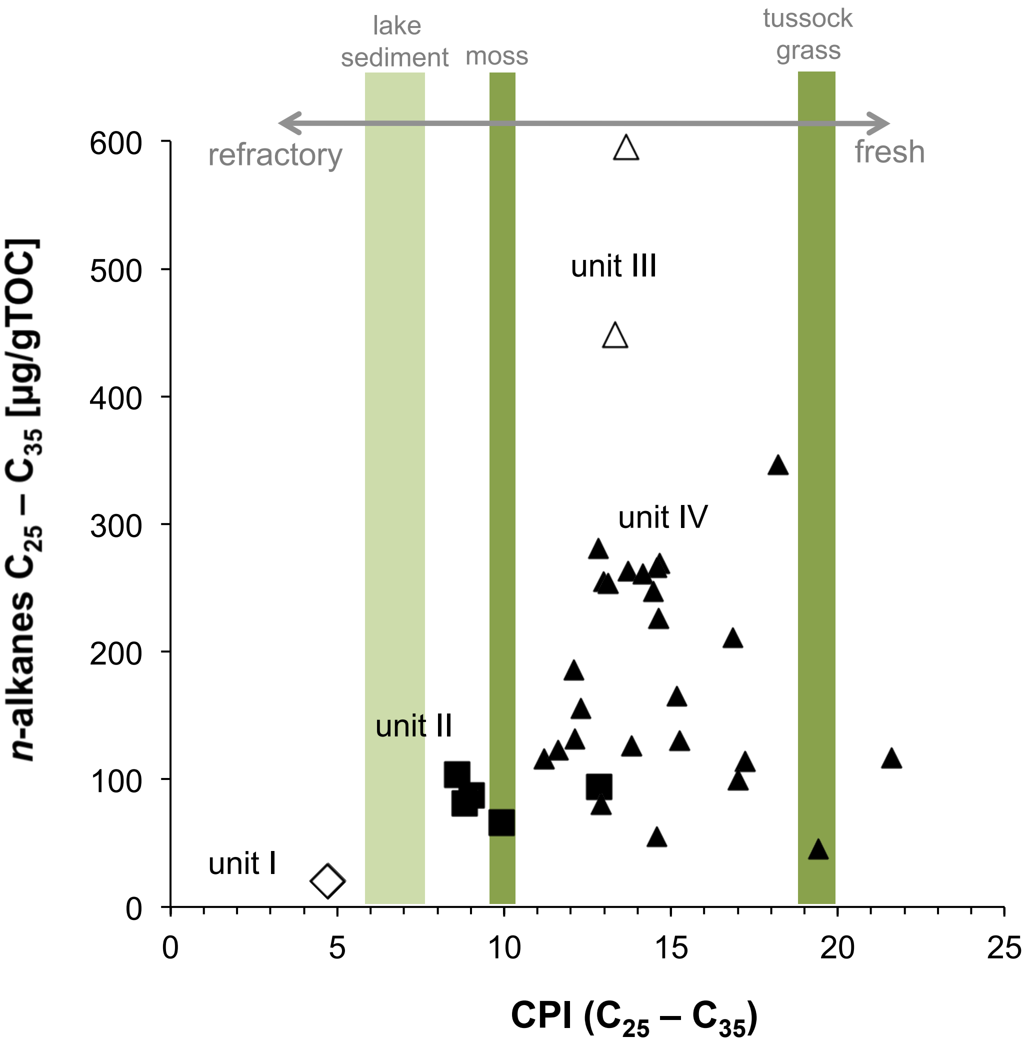

Figure 6

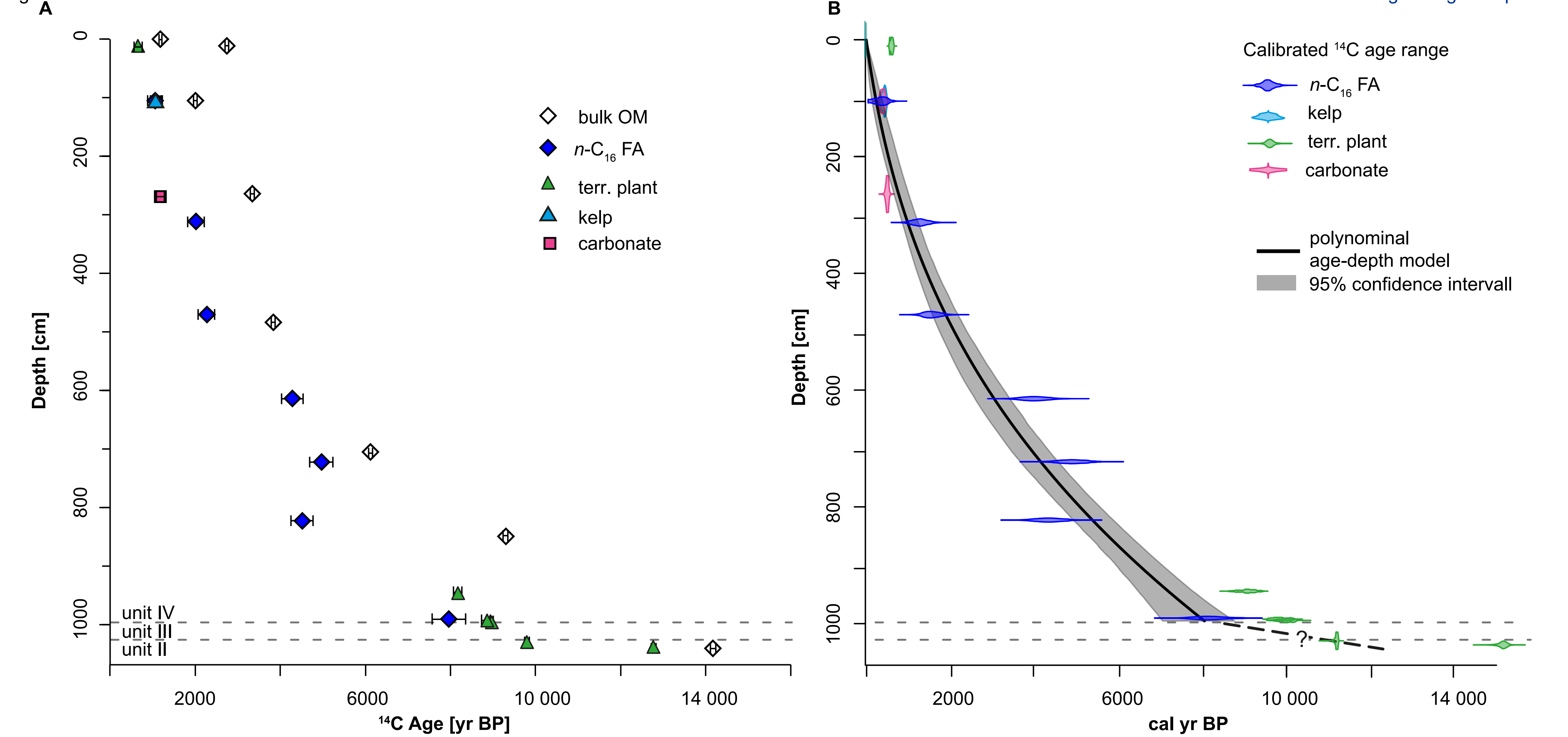

A
Depth [cm]
0
200
400
600
800
1000
unit IV
unit III
unit II
2000
6000
10 000
14 000
14C Age [yr BP]
bulk OM
n-C16 FA
terr. plant
kelp
carbonate
B
Depth [cm]
Calibrated 14C age range
n-C16 FA
kelp
terr. plant
carbonate
polynominal
age-depth model
95% confidence intervall
?
cal yr BP

Figure 7 Click here to download Figure Figure 7.pdf

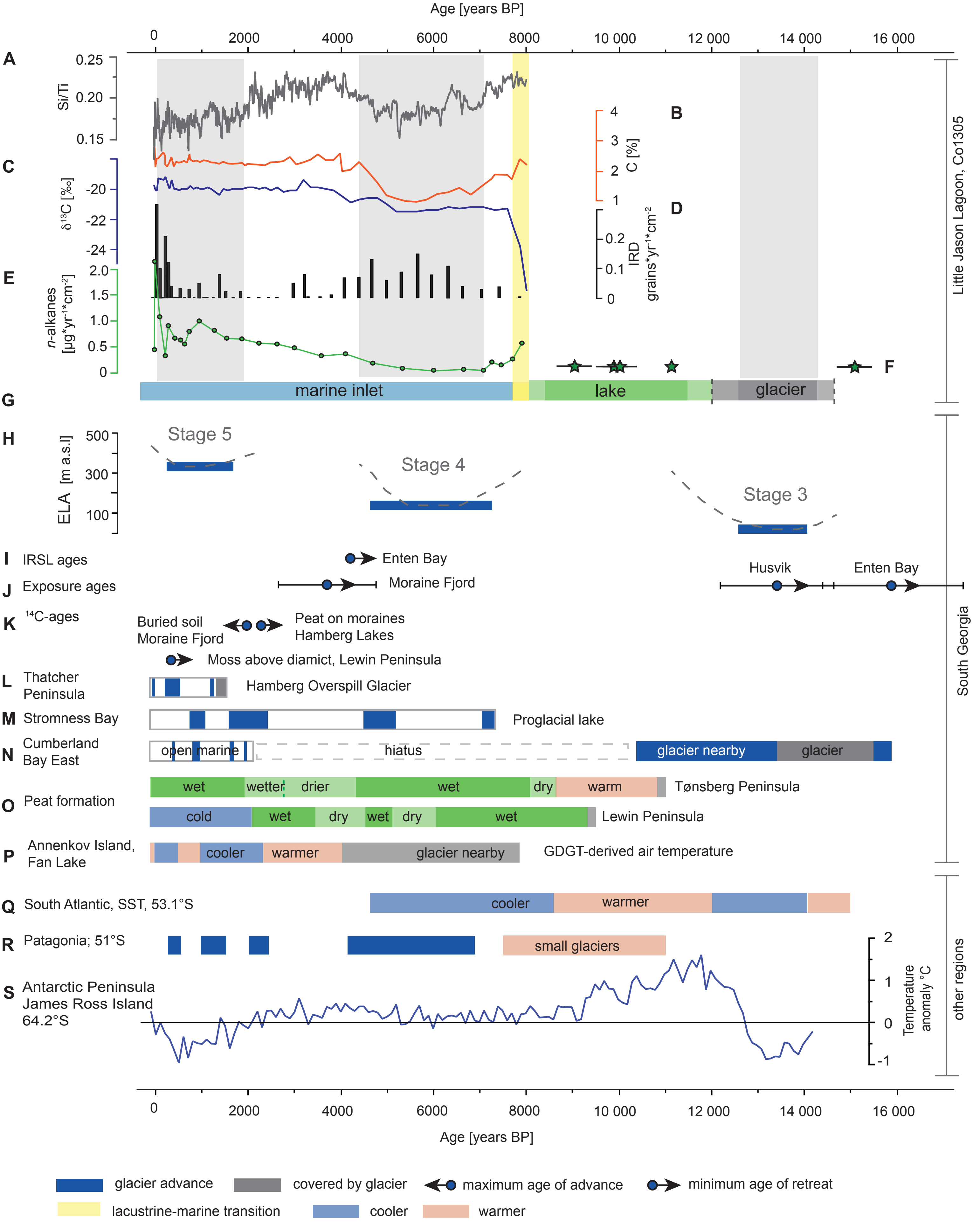

Table 1

AMS Lab No	**Depth [cm]**	**dated material**	**pmC**	**^{14}C age [^{14}C yr BP]**	**^{14}C age corr. [^{14}C yr BP]**	**cal yr BP (2σ range)**
COL2894	2-4	bulk OM	86.2±0.4	1190±45	-	-
COL2362	10-12	bulk OM	70.9±0.4	2760±40	-	
COL2363	105-107	bulk OM	77.9±0.4	2000±45	-	-
COL2364	264-266	bulk OM	66.0±0.4	3340±45	-	-
COL2365	483-485	bulk OM	62.1±0.4	3830±45	-	-
COL2366	707-709	bulk OM	46.7±0.3	6120±50	-	-
COL2541	848-850	bulk OM	31.4±0.2	9300±55	-	-
COL2540	1040-1042	bulk OM	17.1±0.2	14170±70	-	-
COL3942	103-108	*n*-C_{16} FA	88.2±1.8	1005±170	285	0-545
COL3944	308-313	*n*-C_{16} FA	77.95±1.8	2000±190	1280	875-1650
COL3946	468-472	*n*-C_{16} FA	75.1±1.8	2255±200	1535	1120-1950
COL3948	612-617	*n*-C_{16} FA	58.7±1.8	4275±240	3555	3375-4600
COL3950	720-725	*n*-C_{16} FA	54.0±1.8	4955±260	4235	4230-5530
COL3952	820-825	*n*-C_{16} FA	56.9±1.8	4535±250	3815	3665-4960
COL3954	988-993	*n*-C_{16} FA	37.1±1.8	7970±380	7250	7435-9005
COL2359	10-12	plant (terr.)	92.1±0.4	660±40	-	550-655
COL2360	105	kelp (marine)	87.4±0.4	1080±40	360	300-480
COL2839	944-946	moss (terr.)	36.2±0.6	8170±130	-	8690-9420
COL2840	992-994	moss (terr.)	33.3±0.4	8830±100	-	9555-10155
COL2841	994-996	moss (terr.)	32.8±0.4	8970±110	-	9660-10250
COL2210	1029-1031	moss (terr.)	29.53±0.5	9800±40	-	11120-11245
COL2842	1034-1036	moss (terr.)	20.4±0.2	12770±60	-	14865-15370
COL2305	105-107	carbonate	87.7±0.5	1055±45	335	285-460
COL2306	264-266	carbonate	86.4±0.5	1180±40	460	420-545
COL2286	Grytviken	carbonate	91.4±0.5	720±40	modern	-

	Sample depth (cm)	**1034**	**1018**	**1002**	**986**	**922**	**874**	**746**	**602**	**408**	**314**	**186**	**43**
	Concentration (mv/g)	**1.81843**	**1.27443**	**18.0205**	**170.665**	**243.117**	**116.151**	**303.77**	**191.659**	**156.628**	**289.335**	**112.465**	**250.707**
Taxa	**Habitat***												
Fragilariopsis spp.	m		0.5			2	1		0.5	2.5	0.5		
Chaetoceros rs	m	1	3	1	155	254	248	407	360	285	400	253	251
Chaetoceros veg.	m					11	5	5	6	6	23	6	15
Nitzschia spp.	m	1		1			2.5		1.5		0.5		
Minidiscus spp.	m							2	3	4	3		
Odontella spp.	m						2	5	3		2		
Thalassiosira spp.	m	2	4	6	10	3	10	5	3	2	12	12	
Marine (other)	m	1	2	10	13	5.5	4	2	6	6	3.5	5.5	2
Achnanthidium minutissimum	f	4	1	7									
Amphora veneta	f	1	1	7									
Craticula sp.	f	1		1									
Cymbella cistula	f	3	2	5									
Diploneis sp.	f	8	4	98									
Discostella stelligera	f	36	23	20									
Fragilaria capucina	f	4	8	3									
Fragilaria germainii	f		1	0	3								
Fragilaria tenera	f	5	9	0									
Gomphonema affine	f			1									
Staurosirella pinnata	f		1	0									
Synedra sp.	f	1		0									
Fresh (other)	f	5	5	9	8								
Navicula spp.	mbb			1	2	8.5	5.5	7.5	2.5	17	14.5	7	5.5
Nitzschia cf *palea*	mbb				10								
Nitzschia spp.	mbb				11					3.5			
Cocconeis spp.	mbb	3	3	6	6	8	14	7	10	18	11.5	10	1.5
Pseudogomphonema sp.	mbb				2	2		5	3.5	3.5	7	2.5	
Mastogloia sp.	mbb				9								
Opephora spp.	mbb	3	2		17								
Planothidium spp.	mbb	6	1	5	6	1			1			1	4.5
Pseudostaurosira spp.	mbb	31	28	119	60								
Tabularia spp.	mbb				3	6	11	0.5	10.5	12.5	9	14.5	10.5
Marine Benthic/Benthic (other)	mbb	0	0	0	5	1	4	2.5	1.5	2	0	1.5	4.5
Total		**116**	**98.5**	**300**	**320**	**302**	**307**	**448.5**	**412**	**362**	**486.5**	**313**	**394.5**

* f - fresh water; m - marine; mbb - marine benthic &/or brackish

Table S1: List of diatom species identified in 12 samples from core Co1305. Diatom concentrations were calculated using the following equation

$$\boldsymbol{diatom\ concentration} = \frac{((\boldsymbol{NB})(\boldsymbol{AF}))}{\boldsymbol{M}}$$

where N is the total number of diatoms counted, B is the total settling area (mm^2), A is the length of transect(s) counted (mm), F is the diameter of the field of view (mm), and M is the mass of dry sediment used (g).